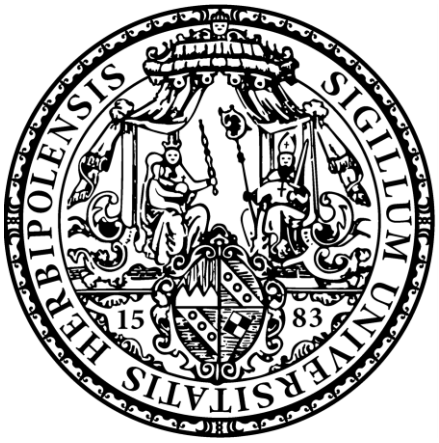

Myocardial B-cell infiltration following occlusion of the left anterior descending artery in mice is driven by CXCL13

Die Infiltration des Myokards durch B-Lymphozyten nach Ligatur der linken Koronararterie im Mausmodell wird durch CXCL13 verursacht

Doctoral thesis for a doctoral degree

at the Graduate School of Life Sciences,

Julius-Maximilians-Universität Würzburg,

Section Biomedicine

submitted by

Susanne Margarete Heinrichs

from

Frankfurt am Main

Würzburg 2018

Submitted on:

28/03/2018

Members of the Promotionskomitee:

Chairperson: Prof. Dr. med. Peter Heuschmann

Primary Supervisor: Prof. Dr. med. Stefan Frantz, Würzburg

Supervisor (Second): PD Dr. med. Niklas Beyersdorf, Würzburg

Supervisor (Third): PD Dr. med. Ulrich Hofmann, Würzburg

Date of Public Defence:

02/08/2018

Date of Receipt of Certificates:

The doctoral candidate is an approbated physician.

Für Mama und Papa

Index

1. Introduction

A watchful immune system is a unique feature of human life. Compared to other living organisms, humans probably have the most sophisticated immune system making their bodies defensive against all kinds of pathogens such as bacteria, viruses, fungi and protozoa. The immune system comprises a complex and flexible network of cells, humoral factors and cytokines located in primary to tertiary lymphoid organs and circulating in the blood.

Of course, like any other cellular system, the immune system can become defective resulting in, for example, either an insufficient defense or in an overshooting reaction directed against endogenous targets.

In immunology, we systematically discriminate between two arms of immunity: On the one hand the innate or non-specific, on the other hand the adaptive or specific immunity. Both arms interact[1] and can be subdivided again into a cellular and a humoral component, the latter consisting of soluble factors (plasma proteins, antibodies) that are able to recognize, bind and inactivate pathogens such as harmful bacteria or viruses. The cellular component encompasses all kinds of immune cells[2].

It has been known for a very long time that natural constitutional variabilities (e.g. genetic modifications) as well as acquired alterations in the immune system (e.g. splenectomy) modify the immune system's effectiveness, potentially resulting in life-threatening medical conditions[3]. This is especially relevant for infectious diseases, where immunodeficiency induced by human immunodeficiency virus (HIV) can, for example, lead to Kaposi sarcoma, a neoplasia caused by an infection with human herpes virus 8 (HHV-8)[4]. But also in other diseases such as cardiovascular diseases, among them ischemic heart disease and stroke, which are still the leading death causes worldwide[5], the immune system plays a critical role and influences the course of disease progression. Today, most scientists and clinicians agree that, to a certain extent, those diseases are also of inflammatory origin as already described e.g. in atherosclerosis[6]. Inflammation

in this context refers to sterile inflammation, i.e. inflammation and immunoreaction without infection[7].

Sterile inflammation has for several years been an interesting field of research also in other cardiovascular diseases. In our research, we focused on its role in acute myocardial infarction (MI) as *heart attack* is still the most frequent death cause in Germany[8].

For many years, there have been various types of prophylactic and therapeutic approaches to treat myocardial infarction, among them anticoagulation, lysis, bypass and, most recently, catheter intervention. As despite of all these treatment options vessel occlusion cannot always be prevented or interrupted early enough, ischemic damage and immune reaction break ground and increase mortality as well as reinfarction rates[9]. In this study, we therefore attempted to investigate myocardial infarction in a mouse model and evaluate the type and extent of damage and repair caused by the immune system with special respect to B lymphocytes, which are already known to play a crucial rule in other inflammatory diseases[10].

1.1. The development of the immune system in humans

The development and maturation of the immune system begin early in fetal life. Pre-B and functional B lymphocytes emerge as early as week nine of gestation in the liver and are dispersed in the blood and spleen by the age of 12 weeks[11].

T lymphocytes develop in the hyperplastic thymus at approximately the same time. They leave the organ after maturation and priming from approximately 14 gestation weeks onwards[12] to populate the spleen and other secondary lymphoid organs.

Secondary lymphoid organs like the spleen are, however, still hypoplastic, mostly due to the lack of antigen stimulus which is required for immune cell proliferation. Until birth,

fetuses do not produce any antibodies of their own. Maternal immunoglobulin G (IgG) acquired through transplacental transfusion helps the immature organism to cope with pathogens while the fetal immune system is still in development[13]. In fact, the IgG production of newborns lags that of adults for up to four to six years after birth. The humoral response to certain antigens is limited until approximately the age of two years, explaining higher rates of infections with certain pathogens (e.g. Streptococcus pneumoniae) in newborns[14].

There is also a small amount of IgA in neonatal humans – possibly also of maternal origin. Own IgA secretion on mucosal tissues does not occur earlier than two to three weeks after birth. As immunization of newborns with bacterial, e.g. capsular polysaccharides, results only in poor antibody production and in very young children a high susceptibility towards certain viral pathogens – among others herpes simplex virus (HSV) and varicella-zoster virus (VZV) is commonly observed, it stands to reason that a newborn's immune system only develops over time and in particular through antigen contact in the first weeks and years of life[12]. Without antigen contact, especially B lymphocytes and plasma cells are apparently still dysfunctional and there is also a lack of precisely fitting T cells.

Antigen procession and pathogen consumption by the so-called innate part of the immune system – for instance through monocytes and macrophages – in contrast, appear to work already by the time of birth[15].

1.2. The development of the immune system in mice

Compared to humans, the murine immune system develops in a slightly different manner. Pluripotent stem cells originating from *blood islets* in the fetal yolk sac start to populate the liver and spleen via the bloodstream around day nine after gestation[16]. Subsequently, the liver hosts hematopoiesis in the mouse embryo. The spleen, as a lymphoid organ, also contributes significantly from day 15 onward, until several weeks after birth, it is, above all, the site of erythropoiesis[17] – and this, unlike in humans, for a life time.

Around birth, when the liver takes over more and more metabolic activity, pluripotent stem cells in both humans and mice emigrate and home to the bone marrow[18]. They settle down in between mesenchymal cells, forming a reticular structure. In mice, B-cell progenitors emerge as early as gestational day 19 in the bone marrow, while T cells can only be detected after birth. Two to four months later, both cells types have reached their maximal numbers. The thymus as a lymphatic organ develops quite early in fetal life, around day nine and ten of gestation, and is shortly afterwards populated by the first, still immature, T lymphocytes from the fetal liver[19]. Those differentiate there until they finally spread as fully competent T-helper and cytotoxic T cells to the periphery. During maturation in the thymus, T-cell receptor (TCR) genes rearrange themselves in the cells and surface expression of variable TCR is made possible.

At that developmental stage, B cells in the mouse are still incapable of producing other immunoglobulin classes than IgM[20]. B lymphopoiesis starts in the fetal liver around day 12 and 13 of gestation. At the same time, a production of B-cell progenitors can be observed in the spleen.

In conclusion, the above-mentioned examples show that developmental stages of, particularly B cells in humans and mice, are, apart from slight differences, comparable. Mouse models are therefore – and not only for that reason, of course – a reasonable model in terms of immunological research.

Of course, there are also some differences one must consider when evaluating results in mouse models. One example is immunosenescence, a progressive impairment of the immune system's function with aging[21] – a process not reproduced in our mouse model.

1.3. The components of the immune system

1.3.1. Innate immunity

The so-called innate immune system is the most native part of defense against pathogens. Pathogens interact with the host via pattern-associated molecular patterns (PAMPs) which are recognized by pathogen recognition receptors (PRRs) on the host's immune cells[22]. PRRs are mainly present on innate immune cells, above all on dendritic cells, macrophages and neutrophils[23]. Prompt identification of PAMPs induces – ideally – an effective immune response due to the involvement of intracellular molecular signaling pathways that unleash a cytokine storm supposed to destroy and eradicate the invading pathogens[24]. For that reason, the innate immune system is the first and, since it reacts immediately, also the fastest barrier against microorganisms.

Belonging to the innate immunity are also the complement system, specific receptors expressed on natural killer cells (NK cells) and the family of toll-like receptors (TLRs) that sense specific microbial molecular structures and are expressed additionally on adaptive immune cells such as myeloid and lymphoid cells[25]. Thereby, innate immunity connects to the adaptive immune system, especially to B and T lymphocytes as well as dendritic cells (DC). Those are primed to react antigen-specific once they have encountered an antigen processed earlier by innate immune cells. TLRs are very important PRRs and probably the most widely studied class.

While ten different TLRs are currently known in humans, there are already twelve that have been described in mice. TLR1 to TLR9 are conserved in humans as well as in mice. TLR1, 2, 4, 5 and 6 are located at the cell surface, recognizing PAMPs from bacteria, protozoa and fungi, whereas TLR3, 7, 8 and 9 are active in intracellular niches, primarily sensing PAMPs derived from deoxyribonucleic acid (DNA) or ribonucleic acid (RNA) of bacteria and viruses[26].

TLR signaling is a complex process involving adaptor molecules like MyD88, TRIF (TICAM-1), TIRAP (Mal) and TRAM[27], which finally activate transcription factors such as nuclear factor kappa-light-chain-enhancer of activated B cells (NF-κB), resulting in the release of pro-inflammatory cytokines and type I interferons, especially in macrophages and DC[28]. When stimulated by microbes or host protein molecule, these cells initiate the formation of a so-called inflammasome, a protein complex that activates caspase-1 and induces inflammation.

Inflammasome activation, e.g. of the NLR family pyrin domain containing 3 (NLRP3) inflammasome, is triggered by pathogens such as the influenza A virus, a negative stranded RNA virus causing severe respiratory illness in humans and animals. In this particular case, the M2 protein, a proton-selective ion channel and virulence factor, is essential for inflammasome activation[29].

TLR4, one of the most widely studied TLRs, is stimulated by lipopolysaccharide (LPS), a thermostable composite of lipids and polysaccharides (esp. lipoglycan) located in the outer membrane of gram negative bacteria. Released upon bacterial infection, LPS acts as an endotoxin and elicits strong immune responses in both animals and humans.

LPS is one of the most widely examined bacterial components stimulating the immune system and causing systemic inflammation and even sepsis if excessive signaling occurs[30]. LPS consists of three parts – namely lipid A, a core oligosaccharide and an O-side chain. Lipid A is considered to be the main PAMP of LPS[31]. It was revealed in 1998 that LPS above all stimulates TLR4. Defects in the Lps gene lead to an in-fact resistance towards endotoxins but to a high susceptibility to uncontrollable infection with gram-negative bacteria because an effective clearance of the pathogen is impeded[32].

Upon recognition of LPS, TLR4 undergoes oligomerization beyond the cell membrane and activates various other downstream adaptors via its toll-interleukin-1 receptor (TIR) domains.

Of course, B cells are activated and receive signals not only through TLRs, e.g. TLR4, but also through their very own B cell receptor (BCR) or via CD40-CD40L interaction during an immune response[33]. The different possibilities of B-cell activation will be reviewed in the following chapter.

1.3.2. Adaptive immunity

The adaptive immune system is not only more specialized and precise than the innate immune system; it also provides long-term protection mechanisms against reinfection. Of course, immunological memory responses – like after vaccination – are favorable, but not always induced.

In contrast to the innate immune system outlined above, adaptive immunity can be described as a flexible and dynamic system of interacting cells, a *community* that can learn and improve. A highly complex response, far beyond mere and undirected immunologic instinct, also demands more resources, resulting in a time delay of several days. This is, because it takes numerous steps until, for instance, highly effective T lymphocytes have developed out of naive T cells and until B cells have expanded and differentiated to secrete proper antibodies. As mentioned before, this is only feasible through the contribution of the innate immune system providing co-stimulation of lymphocytes with molecules induced and presented on cells such as macrophages, for example. Paving the way for the adaptive immune system are also the cytokines, mostly secreted in the early phase of defense predominated by innate immunity.

In the context of adaptive immunity, mucosal immunity is especially important and includes e.g. the clearance of harmful microorganisms at the external borders of the body in the airways, the gut and the urogenital system. At the same time and in that same area, immunological tolerance is needed as not all environmental and potentially allergic agents (e.g. in foods) *must* induce an immune reaction[34]. Inappropriate reactions, e.g. diarrhea or laryngeal edema, are generally referred to as intolerances or allergies.

Schematically speaking, the course of infection can be divided into different steps. After adherence and penetration of the epithelial barrier (e.g. of mucosal tissues) by the infectious agent, innate immune cells initiate a local response to the pathogen to help enclose the lesion. Antigens are incorporated, carried to the responsible lymph nodes and processed there to finally initiate an adaptive immune response including specific antibody secretion by plasma cells, T-cell dependent macrophage activation and mobilization of cytotoxic T cells to the site of infection[35].

In a way, adaptive immune response differs according to the type of agent threatening the integrity of the organism. For example, viruses are first and foremost attacked by $CD8^+$ cytotoxic T cells[36], while most bacteria are opposed by $CD4^+$ T-helper cells in combination with B cells.

B lymphocytes are, in their activation during inflammation, dependent on the aid of T cells, mainly so-called $CD4^+$ helper T cells. B cells carry on their surface various immunoglobulins presenting specific antigens. If these antigens are recognized by T cells with their TCR, those become activated and in turn reactivate B cells, via two different mechanisms[37]. First, T helper cells secrete lymphokines acting as growth and differentiation factors on B cells. If crosslinking of immunoglobulins occurs on the membrane of B cells, responsiveness towards e.g. interleukin 4 (IL-4) can be elevated. At the same time, the IL-2 receptor is upregulated on the cell surface as well as class II major histocompatibility complex (MHC) molecules, adhesion molecules and costimulatory factors[38].

Secondly, there is the so-called contact help activity addressing a tight, direct communication of B and T cells making a directed secretion of helper lymphokines towards the B cell possible[39]. One of these lymphokines is apparently IL-4, a very versatile cytokine known as an important factor for B-cell differentiation, e.g. into plasma cells, for immunoglobulin class switch and MHC II expression on B cells. Besides, IL-4 is also required for further IL-4 production in T cells themselves[40].

Worth mentioning is also the interaction of the molecule CD40 on B cells with its ligand CD40L on T cells. During inflammation, CD40L is transiently expressed by T cells and other non-immune cells and activates B cells to proliferate and secrete immunoglobulins of different classes. Additionally, CD40-CD40L interaction is also of importance in the development of germinal centers and induces survival of B cells. Notably, B cells are also able to express CD40L and can even secrete a soluble form of the ligand. Thereby, they might be able to self-control antibody production[41].

1.4. Regulatory components of the immune system

The immune system – both its innate and adaptive components – can be modulated by various elements such as cells or cytokines.
Concerning the cellular response, a special $CD4^+$ and $CD25^+$ T cell subtype is in the focus of recent research: Regulatory T cells (T_{reg} cells). In contrast to conventional T cells, regulatory T cells are positive for Foxp3 (forkhead box protein P3), a transcription factor necessary for the expression of special, T_{reg}-specific proteins[42].

Foxp3 is essential for the development of T_{reg} cells as well as for the exertion of their inhibitory functions. Foxp3 can, depending on its state of acetylation, either operate as a transcriptional repressor or activator of several genes. It influences not only the T_{reg} lineage but is also responsible for expansion and function of conventional T cells[43]. It diminishes the release of cytokines IL-2 and IFN-y by negative regulation, for instance[44].

Foxp3 also upregulates cytotoxic T lymphocyte-associated molecule 4 (CTLA-4) – also known as CD152 – on regulatory T cells resulting in an inhibition of other T cells as it encodes a T-cell-suppressing protein. Foxp3 additionally inhibits the differentiation of IL-17 producing T helper cells (Th17) by antagonizing RAR-related orphan receptor C (RORC) function. It thereby leads to a down-regulation of IL-17 expression, favoring T_{reg} development[45].

Of course, there are several other known and unknown implications of Foxp3 in T-cell homeostasis.

T_{reg} cells are of importance in maintaining an immunological tolerance by modulating various immune responses. T_{reg} cells derive from $CD4^+$ T helper cells, as do many other T cell subtypes[46]. Th1 cells which are essential for the effective defense against intracellular bacteria or other pathogens develop under the influence of IFN-γ and IL-12, whereas Th2 cells are stimulated as a response to IL-4 and protect against parasites in particular[47]. The only recently discovered Th17 cells seem to oppose extracellular microbes, fungi and yeast. They differentiate in the presence of IL-6 and TGF-γ[48].

T_{reg} cells exert many different effector functions in immunoregulation. They are, as described above, able to upregulate CTLA-4, a protein responsible for limiting overstimulation of T cells. Besides, they produce antiinflammatory factors such as IL-10 and TGF-β. Depending on the localization and local environment, i.e. the context of inflammation, T_{reg} cells show a different phenotype and behavior respectively.

1.5. The role of immunity in myocardial infarction, sterile inflammation

Immune response in myocardial infarction is a *double-edged sword*. While for the healing process after myocardial infarction immune cells are physiologically required, a pathologically prolonged and misdirected immune reaction is liable for adverse

ventricular remodeling in the long run[49]. Regulating and balancing out the system of immune function is necessary to prevent long-term ramifications of myocardial infarction such as impaired contractility and cardiac function resulting in terminal heart failure. To enhance chances for the patient, it is crucial to understand the mechanisms of autoimmunity after MI and spot points of vantage for immune therapy at the same time. Interestingly, a study with patients suffering from chronic heart failure (NYHA II-IV) has recently revealed that non-specific immunomodulation could be beneficial in terms of hospitalization rates and cardiac death[50].

Ventricular remodeling contributes most to chronic infarct-associated heart failure, mainly because it involves pathophysiological processes of reconstruction and reorganization such as infarct enlargement, alterations in the cardiomyocyte union and alterations of the left-ventricular overall geometry and pumping function. Ventricle function is tremendously impaired as the non-infarcted region also experiences lengthening and dilatation that is allegeable with a secondary, potentially progressive hypertrophy due to volume overload[51].

Persisting ischemia, e.g. when timely reperfusion is missed, ventricular overload and neurohumoral overcompensation also contribute to the process of remodeling[52]. Most pharmaceuticals used in the context of myocardial infarction target processes of adverse remodeling. Good examples are angiotensin-converting-enzyme (ACE) inhibitors such as captopril, enalapril and ramipril that reduce the amount of angiotensin type II in the circulation. Therapy with them leads – in addition to the attenuation of the remodeling processes – to vasodilation and thereby blood pressure lowering. It also decreases aldosterone levels, downregulates the sympathetic nervous system and increases perfusion of the renal arteries[53].

Because of their multiple efficiencies, ACE blockers verifiably reduce mortality and are, furthermore, nephroprotective which is especially important with respect to the cardio-renal syndrome. Despite elaborate pharmacotherapeutic approaches, the ventricular remodeling still cannot be controlled effectively. Demand for a not merely symptomatic

but highly specific and easy-to-fine-tune therapy is therefore high. A carefully targeted immunotherapy would probably be able to provide this.

1.6. The kinetics of immune cell accumulation and the role of adaptive immune mechanisms in myocardial infarction with special respect to T and B lymphocytes

It has been known for a long time that concerning sterile inflammation after myocardial infarction in the murine heart, the innate immune system plays an important role. Due to the deficiency of oxygen, numerous cardiac resident cells – not only cardiomyocytes but also cells of the extracellular matrix (ECM) such as fibroblasts or endothelial cells – are damaged. They are either affected to a degree resulting in the release of danger signals or they die immediately. The first phase after myocardial infarction is dominated by proinflammatory cells. Neutrophils are believed to be the first arrivals after an ischemic injury, peaking on day three. At the same time, monocytic cells – especially monocytes – arrive and are apparently the largest group in cell count[54]. Around day four after infarction, inflammation is resolved to a certain extent and the immune response shifts towards a more antiinflammatory and reparative one. This shift is apparently essential for wound healing and initiated by regulatory T cells[55].

Innate immune cells might be the first and most basic-defense cells to arrive. As has been published in several papers in the meantime, there is also an influx of cells numbered among adaptive immunity such as T and B lymphocytes.

Th1 and regulatory T cells are, in any case, the most important $CD4^+$ positive T-cell subset after MI. Th2 and the so-called Th17 cells – IL-17 producing effector T helper cells seemingly especially necessary for pathogen clearance at mucosal barriers[48] – are only

of minor importance. According to several publications, other T-cell subsets ($CD8^+$ T cells, NK T cells), NK cells and B cells peak on day seven after myocardial infarction.

If reperfusion can be initiated early enough, the absolute number of leucocytes infiltrating the heart declines and the immune processes are altered as well: Innate immune cells are activated much earlier, the adaptive immune system's reaction is weakened. In the clinical setting of humans suffering from acute myocardial infarction this seems to be beneficial.

Still, many scientists agree that there is also something referred to as the *reperfusion injury*. The term refers to a progressive cell damage including necrosis, apoptosis and autophagocytic mechanisms as well as the activation of the immune system and the influx of immune cells. It occurs, even if an occluded coronary artery can be reopened on time. Some of the effects can be explained by the extensive hyperemia during reperfusion.

B lymphocytes accumulate in the heart after myocardial infarction. This has been shown simultaneously to our discovery by a French group[56]. Currently, not much is known about the phenotype of these B cells. It is, however, disputable, if many of these B cells – among them some cardiac resident B cells – can secrete antibodies, i.e. are plasma cells. This suggests a role of B cells acting as an intermediary between innate and adaptive immunity. B lymphocytes are highly present already in the steady-state heart, as they are the second largest group of cardiac-resident leucocytes. Usually, almost 150 cells per mg heart tissue can be found in mice. Antigen presenting cells (APC), which are positive for CD11b, CD11c, F4/80 and MHCII, are the largest group of immune cells with approximately 1750 cells per mg, the third largest group are monocytes[57]. This already indicates the importance of innate immunity for the healthy, unchallenged heart.

In cardiovascular diseases, some findings point out that a containment of the immune reaction and especially the limitation of the B-cell response might be beneficial. One review summarizes that, considering several recent publications, a depletion of B cells through anti-CD20 specific antibody treatment seems to result in reduced atherosclerosis, mainly because mature B cells are cleared while beneficial B1 B cells

persist. Apparently, the depletion of B cells also results in less activated dendritic cells (DC) and T cells, whose accumulation was also partly inhibited[41]. Cytokine secretion patterns of these T cells were also altered: Levels of INF-y, which is atherogenic, were lower. IL-17A, however, was increased while its neutralization cancelled out the favorable effects of B-cell depletion on atherosclerosis. IL-17, secreted by Th17 cells, $CD8^+$ T cells, neutrophils and others, is most likely important in regulating local tissue inflammation via cytokines and chemokines.

In conclusion, these findings suggest that B cells contribute to the development of atherosclerosis in mice by modulating T cell activation and recruitment as well as cytokine production[58].

Additionally, one can imagine that a depletion or inhibition of B cells might just as well be beneficial in myocardial infarction.

1.7. Therapeutic immunomodulation in healing and remodeling after myocardial infarction

Considering what is already known about the role of the immune system in cardiovascular diseases and especially in myocardial infarction, there are several possibilities to interfere with the system therapeutically.

Supposing that cardiac antigens are released in the heart tissue after a period of ischemia and there is presentation of these antigens involving various immune cells afterwards, one idea is to vaccinate individuals at risk with the relevant cardiac antigens prophylactically. The concept of oral tolerance – the ingestion of a heart-tissue extract, and consecutive development of immunological tolerance against cardiac antigens – could help contain myocardial damage and improve healing after myocardial infarction, Ramos et al. argue[59]. They induced myocardial damage in Wistar rats with subcutaneous

injections of isoproterenol, a derivate of noradrenaline and, unlike noradrenaline, a non-selective β-adrenergic agonist. Stimulation of β receptors activates the intracellular adenylate cyclase, converting adenosine triphosphate (ATP) to cyclic adenosine monophosphate (cAMP) which then activates protein kinase A (PKA) phosphorylating calcium ion channels. Applied systemically, isoproterenol thereby results in increased heart contractility and heart rate and a lowered blood pressure and is therefore used in the therapy of bradycardiac arrhythmias. In the lung, it leads to a relaxation of smooth muscle cells in the bronchi. Besides, it prevents the secretion of anaphylactic mediators such as histamine from mast cells, qualifying it as a drug against allergic asthma, too[60]. High doses of isoproterenol are, however, cardiotoxic and induce ischemic injury, just like myocardial infarction does[61]. Wistar rats were observed concerning the cardiac healing process after ischemic damage for 60 days. Ramos et al. assessed cardiac function by performing Langendorff experiments. Additionally, they examined the heart-draining lymph nodes in the mediastinum of the animals and evaluated the lymphocytes' expression patterns. These lymphocytes apparently showed a proinflammatory and profibrotic profile, as they expressed TNF-α, INF-γ and CCL-5.

The group from Florianópolis in Brazil found that if the laboratory animals were *primed* prior to the isoproterenol injection with a heart lysate delivered orally by gavage feeding (minimal effective dose: 20 mg), the respective lymph nodes did, however, not expand. In mediastinal lymph nodes as well as the drained heart tissue, overall cytokine and chemokine levels were reduced. In the tissue, antiinflammatory $Foxp3^+$ was expressed much earlier (already on day three) than in the other group, hinting at an earlier influx of antiinflammatory regulatory T cells (T_{reg} cells). Besides, signs and markers of inflammation occurred less frequently and collagen deposition, which usually has a negative effect on the heart function, was reduced.

These results indicate that the induction of oral tolerance with cardiac antigens might help to contain remodeling and impeded heart function after MI. Myosin, actin and tropomyosin are promising protein candidates to be responsible for immunization against myocardial injury as they have been proven to induce immunological activation

ibidem[52]. Ramos et al. speculate that the protein inducing oral tolerance may, more specifically, indeed be the cardiac isoform of the myosin heavy chain or even cardiac troponin.

Recent publications support the idea that the induction of antigen-specific mucosal tolerance could help suppress inflammation and immunity. Its effectiveness was shown in experimental autoimmune myocarditis as well as myocardial infarction by researchers from Heidelberg and Cologne in 2011. In this case, the antigen cardiac troponin I (cTnI) was applied intranasally and significantly improved heart function, measured by echocardiography[62].

Frenkel et al. had described even earlier, in 2009, that mucosal immunization directly affects T-cell response and is also beneficial in an ischemia-reperfusion model. T cells activated by nasally administered proteins such as cardiac troponin tend to show an antiinflammatory phenotype secreting IL-10 and TGF-β. More precisely, these T cells were described as $CD4^+$ and could possibly be regulatory T cells.

In this study, C, I and T troponin were applied as a vaccine. Treated animals showed considerably smaller infarct sizes potentially due to a minimized immune reaction[63]. Other possibilities to improve the outcome after myocardial infarction comprise methods such as depletion of immune cell subsets or certain chemokines.

1.8. Rationale and intention of the study

Cardiovascular diseases are the most frequent cause of death in Germany. In 2012, more than 40 % of all deaths were caused by myocardial infarction, heart failure or sudden cardiac death. Especially cardiac disease is elevated in elderly people. 92 % of deaths from cardiac diseases were at least 65 years old. Myocardial infarction appears to be a

disease which tends to affect more males than females, about 56 % of dead were male and 44 % were female in 2012[8].

Apart from the direct ramifications of myocardial ischemia, there are plenty of minor and major complications, comorbidities and side effects crucially affecting the patient's mortality. Several factors influence direct outcome, e.g. frequencies of ventricular rupture as well as long-term survival, mainly determined by adverse remodeling. Among them are other illnesses like connective tissue diseases, for instance, method of therapy and concurrent medication like antidepressant agents, which seem to deteriorate healing by influencing matrix metalloproteinase 13 (MMP13) und matrix functioning[64]. Of course, this is only one example elucidating the importance of immunity in myocardial infarction.

After myocardial infarction, the immune system is activated and regulates wound healing and scar formation through secretion of messenger substances, the so-called cytokines. While in that context, a lot is known about innate immunity[65], the responsibilities of the adaptive immune system are still not well studied. While more is known about T cells[66,26], B lymphocytes are more or less a *black hole* – although preliminary tests revealed that there are approximately four times more B than T lymphocytes in the naive heart. The interaction of innate and adaptive immunity is also obvious in B cells, which indeed belong to the so-called adaptive and highly-specific *arm* of the immune system, but are activated by the innate immune system which allocates them a kind of linker function. It is already known that B cells are of importance in healing processes, for example in the skin[67]. By contrast, B cells also play a role in several autoimmune diseases such as rheumatoid arthritis where they contribute to tissue injury and destruction[68].

In the heart, some scattered B cells are found even in the steady-state, i.e. in the undamaged heart under physiological conditions. After myocardial infarction, which we experimentally model in mice, we could demonstrate that B lymphocytes accumulate in the early phase after tissue injury between day one and day seven. Therefore, B cells could be of importance in healing and remodeling processes in the myocardium. To

describe their role and function in both these mechanisms more exactly, we attempt to investigate mice undergoing permanent ligation of the left anterior descending artery (LAD), especially focusing on structural changes in the extracellular matrix with molecular methods such as polymerase chain reaction (PCR) and immunohistochemistry and investigating alterations in inflammatory reactions predominantly with fluorescence-activated cell scanning (FACS). Investigations have been chosen to generally take place at different time points, in concrete terms on day one, day three, occasionally day five and day seven.

Our study addresses the role and function of B lymphocytes in myocardial infarction. We attempt to reveal and explain the mechanisms responsible for B-cell infiltration of the damaged myocardium and want to outline B lymphocytes' assignment in between the poles of innate and humoral immunity. B cells are generally recognized by their capacity to produce antibodies of different isotypes against specific foreign antigens. In the context of autoimmune diseases, B lymphocytes, however, also contribute to etiopathogenesis because they produce self-reactive antibodies against endogenous, innocuous antigens. Opsonization of pathogens and complement fixation also belong to B cells' very own tasks. In the last years, nevertheless, the efficiency of B cells in producing a wide range of cytokines has become another focus of attention. In an antibody-independent way they produce pro-inflammatory cytokines such as IL-2, IL-6, IL-17, IFN-α, IFN-γ, TNF-α and lymphotoxin (LT), as well as antiinflammatory factors like IL-4, IL-10 and TGF-β[69]. In a way, B cells thereby modulate both innate and adaptive components of the immune system and simultaneously exercise pathogenic and protective roles in immunological reactions and disorders. My aim was to assess damages and duties of B cells in myocardial infarction and to highlight opportunities that shape and modify specific reactions in the myocardium.

2. Material and Methods

2.1. Material

2.1.2. Reagents

2.1.2.1. Chemicals and drugs

Denomination	Manufacturer
4-fold SDS loading buffer	LI-COR (Lincoln, USA)
Acrylamide 30 %	Carl Roth GmbH + Co. KG (Karlsruhe, Germany)
Ammonium persulfate (APS)	Sigma-Aldrich Chemie (Steinheim, Germany)
Aqua ad injectabilia	B. Braun Melsungen AG (Melsungen, Germany)
Aqua dest.	-
Buprenorphin: Buprenovet®, 0,3 mg/ml	Bayer (Leverkusen, Germany)
Disinfecting agent: Terralin® liquid (containing 94 % ethanol and propan-1-ol)	Schülke & Mayr GmbH (Norderstedt, Germany)
Entellan®	Merck Millipore (Darmstadt, Germany)
Eosin	Merck Millipore (Darmstadt, Germany)
Ethanol	Chemsolute®, Th. Geyer GmbH & Co. KG (Renningen, Germany)
Hematoxylin	Morphisto GmbH (Frankfurt am Main, Germany)

Heparin-Natrium-25000-ratiopharm	Ratiopharm GmbH (Ulm, Germany)
Isofluran CP®	CP-Pharma Handelsgesellschaft mbH (Burgdorf, Germany)
Isopentane	Sigma-Aldrich Chemie (Steinheim, Germany)
Mowiol 4-88	Carl Roth GmbH + Co. KG (Karlsruhe, Germany)
Sodium chloride (NaCl) 0,9 %	B. Braun Melsungen AG (Melsungen, Germany)
Nonfat dry milk	Cell Signaling Technology, Cambridge, UK
PageRuler™ Prestained Protein Ladder	Thermo Scientific (Waltham, USA)
Picrosirius red	Morphisto GmbH (Frankfurt am Main, Germany)
Ponceau S solution: 0,25 % (w/v) Ponceau S in 1 % (v/v) acetic acid	Sigma-Aldrich Chemie (Steinheim, Germany)
Rotihistol A	Carl Roth GmbH + Co. KG (Karlsruhe, Germany)
Rotihistol B	Carl Roth GmbH + Co. KG (Karlsruhe, Germany)
Sodium dodecyl sulfate (SDS)	Sigma-Aldrich Chemie (Steinheim, Germany)
Tetramethylethylendiamin (Temed)	Sigma-Aldrich Chemie (Steinheim, Germany)
Tris(hydroxymethyl)aminomethane (Tris)	Sigma-Aldrich Chemie (Steinheim, Germany)
Trypan Blue Solution (0,4 %)	Sigma-Aldrich Chemie (Steinheim, Germany)
Xylene	Sigma-Aldrich Chemie (Steinheim, Germany)

β-Mercaptoethanol	Sigma-Aldrich Chemie (Steinheim, Germany)

2.1.2.2. Enzymes and sera

Balanced salt solution/Bovine serum albumin (BSS/BSA)	Institute of Virology and Immunobiology (Würzburg, Germany)
Collagenase Type II (360 U/mg)	CLS 2; Worthington Biochemical Corporation (Lakewood, USA)
Fetal Calf Serum (FCS)	Institute of Virology and Immunobiology (Würzburg, Germany)
Normal goat serum	Vector Laboratories (Burlingame, USA)

2.1.2.3 Buffers, Solutions and Liquids

CAPS Buffer: 10 mM CAPS (pH 11.0) and 10 % (v/v) methanol prepared in 1 l of H_20	AppliChem GmbH (Darmstadt, Germany)
Dulbecco's Phosphate-buffered saline (PBS)	Biochrom AG (Berlin, Germany)
Erylysis Buffer: 150 mM NH_4Cl, 10 mM $NaHCO_3$, and 0.15 mM EDTA; pH 7.4 in H_2O	*in-house production*
FACS Shut-down-Solution	BD Biosciences (Franklin Lakes, USA)
FACS-Clean	BD Biosciences (Franklin Lakes, USA)
FACS-Flow	BD Biosciences (Franklin Lakes, USA)
FACS-Rinse	BD Biosciences (Franklin Lakes, USA)

RPMI	gibco® by Life Technologies GmbH (Darmstadt, Germany)
SDS running buffer: 0.384 M glycine, 50 mM Tris/HCl (pH 8.6), 0.1 % (w/v) SDS	*in-house production*
Strip buffer (mild): 15 g glycerine, 1 g SDS, 10 ml tween; pH 2,2	*in-house production*
TBST: 150 mM NaCl, 10 mM Tris/HCl (pH 7.4), 0.1 % (w/v) Tween-20	*in-house production*

All chemicals that are not further specified were purchased at Sigma-Aldrich Chemie (Steinheim, Germany).

2.1.2.4. Other material

Compensation Beads (Anti-rat and anti-hamster Ig κ)	BD Biosciences (Franklin Lakes, USA)
CountBright™ Absolute Counting Beads	Invitrogen (Carlsbad, USA)
ImmEdge™ Hydrophobic Barrier Pen	Vector Laboratories (Burlingame, USA)
Tissue-Tek®	Sakura Finetek (Torrance, USA)

2.1.2.5. Kits

C&E Version ExpressArt mRNA amplification Pico kit	AmpTec GmbH (Hamburg, Germany)
cDNA Synthesis Kit	iScript™ cDNA Synthesis Kit; Bio-Rad Laboratories (Hercules, USA)
DNase set	DNase 1 Amplification Grade; Sigma-Aldrich Chemie (Steinheim, Germany)
Enhanced Chemiluminescence (ECL) Kit (for Western Blot)	Amersham™ ECL™ Prime Western Blotting Detection Reagent; GE Lifesciences, Little Chalfont, UK
Mastermix	TaqMan® Gene Expression Master Mix; Applied Biosciences (Foster City, USA)
Mouse CXCL13/BLC/BCA-1 Quantikine ELISA Kit	R&D Systems (Minneapolis, USA)
RNeasy Micro Kit	Qiagen (Hilden, Germany)
RNeasy Mini Kit	Qiagen (Hilden, Germany)

2.1.2.6. Biomolecules and compounds

FACS antibodies

anti-	Fluorophore	Cl1	Manufacturer
B220/CD45R	AF 647	RA3-6B2	BioLegend (San Diego, USA)
CD11b	PE	M1/70	BioLegend (San Diego, USA)
CD138	PE	281-2	BioLegend (San Diego, USA)
CD16/32 (TruStain fcX™)	-	93	BioLegend (San Diego, USA)
CD21	FITC	7E9	BioLegend (San Diego, USA)
CD23	PE	B3B4	BioLegend (San Diego, USA)
CD23/Fc epsilonR II	PE/Cy7	EBVCS-5	Biozol (Eching, Germany)
CD45	eFluor®	30-F11	eBioscience (San Diego, USA)
CD5	PerCP	five3-7.3	BioLegend (San Diego, USA)
CXCR5	PE/Cy7	L138D7	BioLegend (San Diego, USA)
GM-CSF	PerCP/Cy5.5	MP1-22E9	BioLegend (San Diego, USA)
IgD	FITC	11-26c.2a	BioLegend (San Diego, USA)
IgM	PE	RMM-1	BioLegend (San Diego, USA)
Ly-6G	AF 647	1A8	BioLegend (San Diego, USA)

Other antibodies

anti-	specificity	linked to	Manufacturer
goat IgG	rabbit (pAb)	HRP	Abcam (Cambridge, UK)
goat IgG	donkey	AF five94	Invitrogen (Carlsbad, USA)
histone H3 (D1H2) XP®	rabbit (mAb)	-	Cell Signaling Technology (Cambridge, UK)

mouse CXCL13 mAb (Cl1 143614)	rat (mAb)	-	R&D Systems (Minneapolis, USA)
mouse CXCL13 pAb	goat (mAb)	-	R&D Systems (Minneapolis, USA)
mouse IgG, IgA, IgM (H+L)	goat	HRP	Abcam (Cambridge, UK)
rat IgG	goat	AF 647	Invitrogen (Carlsbad, USA)

Dyes

4',6-diamidino-2-phenylindole (DAPI)	-	-	Life Technologies GmbH (Darmstadt, Germany)
Phalloidin		AF 488	Sigma-Aldrich Chemie (Steinheim, Germany)

RT-PCR primers

Actb	Mm00607939_s1	TaqMan® Gene Expression Assay, Life Technologies GmbH (Darmstadt, Germany)
CCL19	Mm00839967_g1	TaqMan® Gene Expression Assay, Life Technologies GmbH (Darmstadt, Germany)
CXCL12	Mm0044fivefivefive3_m1	TaqMan® Gene Expression Assay, Life Technologies GmbH (Darmstadt, Germany)
CXCL13	Mm00444five34_m1	TaqMan® Gene Expression Assay, Life Technologies GmbH (Darmstadt, Germany)
GAPDH	Mm9999991five_g1	TaqMan® Gene Expression Assay, Life Technologies GmbH (Darmstadt, Germany)

2.1.3. Utilized devices, equipment and software

2.1.3.1. Devices

Automatic pipette: Pipetboy acu	Integra Biosciences (Fernwald, Germany)
Blotting system: Mini-PROTEAN® 3 Cell	Bio-Rad Laboratories (Hercules, USA)
Centrifuges: Centrifuge 5810 R; Biofuge pico	Eppendorf (Hamburg, Germany); Heraeus Instruments (Hanau, Germany)
ELISA and fluorescence plate reader: Dynex MRX^{e} tc	Magellan Biosciences (North Billerica, USA)
Flow cytometer: FACS Canto II	Becton Dickinson (Heidelberg, Germany)
Fluorescence microscope: Axio Imager.Z1m	Carl Zeiss Microscopy (Thornwood, USA)
Incubator: BB 6220	Heraeus Instruments (Hanau, Germany)
Microcentrifuge	neoLab Migge Laborbedarf-Vertriebs GmbH (Heidelberg, Germany)
Micropistill for 1,5-2,0 ml tubes	Eppendorf (Hamburg, Germany)
Microtome: Leica CM 1850 Cryostat	Leica Microsystems (Wetzlar, Germany)
NanoDrop 2000c	Thermo Scientific (Waltham, USA)
Nitrocellulose membrane: Roti®-NC, 0.2 µm pore size	Carl Roth GmbH + Co. KG (Karlsruhe, Germany)
PCR machine: Biometra T-personal Combi	Biometra (Göttingen, Germany)
pH-meter: WTW pH 91 plus pH electrode SenTix® 21	WTW (Weilheim, Germany)
Pipettes	Eppendorf (Hamburg, Germany)
Refrigerators	Liebherr (Bulle, Switzerland)
RT-PCR cycler: iCycler iQ®	Bio-Rad Laboratories (Hercules, USA)

RT-PCR plates: iCycler iQ® PCR Plates 96-well	Bio-Rad Laboratories (Hercules, USA)
Scales: Sartorius analytic A 120 S	Sartorius AG (Göttingen, Germany)
Surgical instruments	Aesculap/B. Braun Melsungen AG (Melsungen, Germany)
Suture: Silk Black 6/0	FSSB GmbH (Jestetten, Germany)
TC10™ Automated Cell Counter	Bio-Rad Laboratories (Hercules, USA)
Toshiba Aplio ultrasound device	Toshiba Medical Systems (Ōtawara, Japan)
Vortexer: IKA® MS 3 basic	IKA®-Werke GmbH & CO. KG (Staufen, Germany)
Western Blot Scanner (Model: 3600)	LI-COR (Franklin, USA)
Whatman paper	Munktell & Filtrak GmbH (Bärenstein, Germany)

2.1.3.2. Software

Adobe Photoshop®	Adobe Systems GmbH (München, Germany)
Axiovision 4.8	Carl Zeiss Microscopy (Thornwood, USA)
BD FACSDiva™	BD Biosciences (Franklin Lakes, USA)
FlowJo 7.6	FACS Plot Software, Tree Star (Ashland, USA)
GraphPad Prism 6	Statcon (Witzenhausen, Germany)
iCycler	Bio-Rad Laboratories (Hercules, USA)
ImageJ software version 1.44;	National Institute of Health (Bethesda, USA)

Inkscape Version 0.91-1	Software Freedom Conservancy (New York, USA)
Microsoft Office 2010	Microsoft Corporation (Redmond, USA)
Nice software package	Toshiba Medical Systems (Ōtawara, Japan)
ZEN 2011 (blue edition)	Carl Zeiss Microscopy (Thornwood, USA)

2.1.4. Other materials

Glassware, single-use plastics containers like tubes, pipettes etc. were purchased at the following companies:

Falcon (Heidelberg, Germany)

Greiner (Frickenhausen, Germany)

Sarstedt (Nümbrecht, Germany)

Schott Duran (Mainz, Germany)

Sterilin Limited (Cambridge, UK)

2.2. Methods

2.2.1. Animal experimentation

Utilized mice originated from the inbreeding line of C57BL/6N and were purchased from Harlan (Rossdorf, Deutschland).

All experiments with animals were performed according to the provisions of the Protection of Animals Act and were approved by the *Regierung von Unterfranken* in the *Tierversuchsantrag* TVA 64/13.

2.2.1.1. Keeping of animals

Mice were kept in cages with six animals at maximum. Their health status was examined daily by both trained keepers and scientifically experienced personnel. Especially noticeable problems in behavior, evidence for physical or mental pressure and texture of coat were assessed. If abnormalities occurred, mice were either excluded from the experiments or euthanized according to the current legal provisions.

2.2.1.2. The mouse model of permanent myocardial infarction

In our mouse model of acute myocardial infarction, the left coronary artery (LAD) was permanently ligated with a suture to simulate a clinical situation of heart ischemia, where a coronary artery is occluded by a thrombus, e.g. due to atherosclerosis. At first, mice were slightly narcotized with isoflurane in a glass pot. Afterwards, they were intubated with a vein catheterization device connected with a rodent ventilator maintaining deep anesthesia with isoflurane during the whole operation. Mice were

fixed with tape on their back and with extremities abducted on a heated plate to sustain a body temperature of about 37°C and prevent them from becoming hypothermic.

The thorax was disinfected, depilated and afterwards opened at the level of the fourth intercostal space – cutting muscles along the direction of fiber. The thorax was then kept open with a rib spreader. The LAD was circled about 1 mm apical of the left atrium and permanently ligated with a silk suture drawn tight (Figure 1). In sham-operated animals, the procedure was identical except for the ligation of the artery. A silk suture was, however, placed *ibidem*.

Subsequently, the thorax was closed adapting the muscle layers and clipping the skin. For post-operation analgesia, mice received 0,05 to 0,1 mg buprenorphine (Buprenovet®, 0,3 mg/ml, Bayer, Leverkusen, Germany) per kg bodyweight intraperitoneally (i.p.). In our mice, this equated to 300 µl of sodium chloride (NaCl) solution containing 6 µg buprenorphine/ml solution. Meanwhile, inhalation anesthesia with isoflurane was ceased. Mice, however, received ongoing oxygen ventilation until spontaneous respiration was restored.

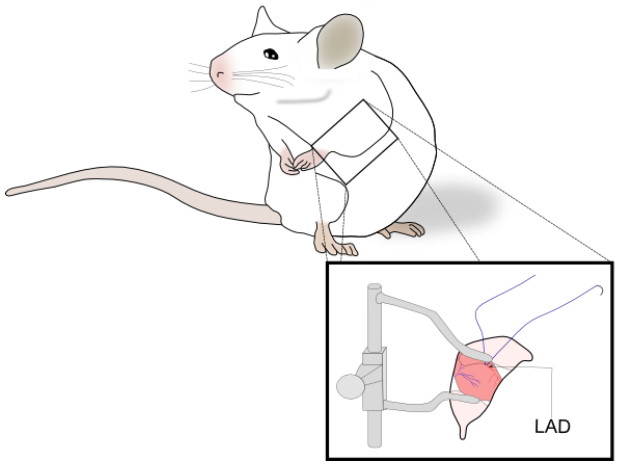

Figure 1: Permanent LAD ligation with a silk suture is performed to simulate myocardial infarction in the mouse.

2.2.1.3. Drug administration

Most drugs in our experiments were administered intraperitoneally. Because the caecum of most mice is located on the left side, injections were performed at the right lower part of the abdomen to prevent defective injections into subcutis, bladder or intestines potentially resulting in organ perforation. During injections, spontaneously-breathing mice were held nuchally to keep them immobilized and incapable of biting.

In some cases, drugs were also injected retroorbitally (r.o.). Mice were intubated and narcotized with isoflurane so that they did not perceive pain and remained calm. Afterwards, the mouse's eye was partially protruded from the socket by applying gentle downward pressure to the skin dorsal and ventral of the eye. We then placed the needle cautiously in the medial canthus at an angle of approximately 30° reaching into the retro-bulbar space behind the globe of the eye and injected slowly without previous aspiration. For more details, see *Retro-orbital injections in mice* by Yardeni et al.[70].

2.2.1.4. Echocardiography

All echocardiographic assessments were done on a Toshiba Aplio system with a 15-MHz ultrasound transducer under spontaneous respiration with additional light anesthesia with isoflurane (≈1.5 vol. %). 24 short axis two-dimensional echocardiographic images acquired at the mid-papillary level as well as apical levels of the LV were stored as digital loops. Left-ventricular (LV) end-systolic and end-diastolic areas had to be calculated afterwards by manual tracings of the endocardial border followed by planimetry with the Nice software package (Toshiba Medical Systems). To determine diameters on papillary (PA) and apical (AP) levels, simultaneous transversal M-mode tracings were recorded with the cursor placed in the middle of the LV cavity.

2.2.1.5. Harvesting of organs

Mice were injected with 0,08 ml Heparin (5,000 IE/ml) intraperitoneally. To ensure a certain degree of sterility, mice were disinfected externally with Terralin® liquid (containing 94 % ethanol and propan-1-ol) to prevent the animal hair from contaminating the situs. Then, the coat was cut and median thoracotomy performed. Diaphragm and ribs were cut and afterwards the thoracic part of the aorta was transected to exsanguinate the animal. The heart was cut out of the mediastinum at its basis und scar and septum were separated on macroscopic examination. To extract the spleen, the peritoneum was opened from the white line. The gastrolienal ligament was cut through and the organ was carefully liberated from the circumjacent fat tissue with blunt anatomical tweezers.

Harvested organs were cleaned, washed and transferred to ice-cold phosphate-buffered saline (PBS) immediately.

2.2.2. Cell biology and molecular biology methods

2.2.2.1. Histology and immunofluorescence microscopy

After organ explantation, organs were embedded in Tissue-Tek® (Sakura Finetek, Torrance, USA) and quick-frozen on dry-ice (submerged with isopentane) and afterwards stored at -80 °C. Slides of 7 µm thickness were prepared with a microtome (Leica CM 1850 Cryostat, Leica Microsystems, Wetzlar, Germany) and stored at -20 °C. Upon use, slides were dried at room temperature for 30 min and afterwards fixated in a cuvette at -20 °C with ice-cold methanol for 10 min and with acetone for 1 min.

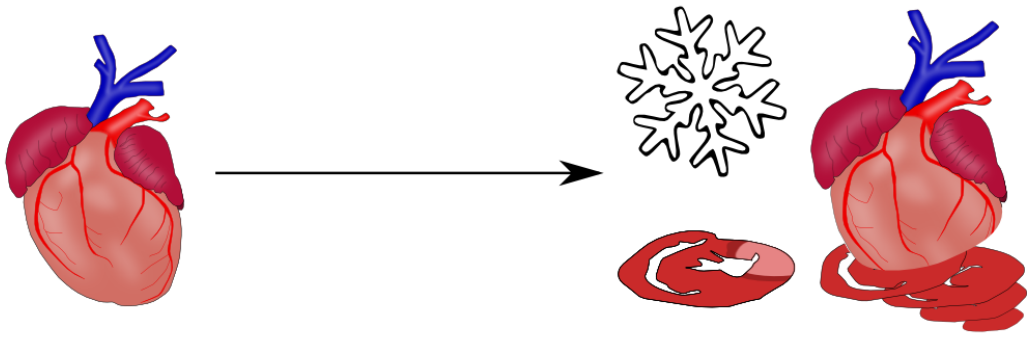

Figure 2: Cryosections are prepared from heart tissue embedded in Tissue-Tek®.

Thereafter, slides were dried at RT again and subsequently washed in PBS for 5 min. The following steps were all carried out in a *wet chamber*. The histological specimens were encircled with a special pen (ImmEdge™ Hydrophobic Barrier Pen, Vector Laboratories, Burlingame, USA). We performed sequential dilution series to determine the adequate concentration of either primary or secondary antibody.

Usually, we covered slides with the primary antibody (25 µl/slide) in a concentration of 0.005 mg/ml (in PBS) and incubated at RT protected from light for 60 min. If specimens were extraordinarily large, they were covered with 50 µl of diluted antibody respectively. Incubation was followed by 3 x 5 min of washing in PBS. Afterwards the secondary antibody was applied (25 µl/slide) in a concentration of 0.01 mg/ml (in PBS) and mixed with 5 % of serum of the respective specificity and incubated for 30 min (conditions like above). After 25 min, DAPI was added (one drop/specimen). Slides were washed again, embedded in Mowiol and covered with a cover slip.

In some experiments, we used phalloidin to stain vital myocardium to distinguish it from the infarct area. Phalloidin (or *phallotoxin*) is originally known as one of the toxins of the fungus death cap (Amanita phalloides)[71], leading to severe intoxication symptoms and delayed hepatic and renal failure (three to four days after consumption) in human beings[72]. Phalloidin's toxic effect is based on its irreversible binding of F-actin

(filamentous actin), thereby causing an arrest of cellular transport. As a dye, we used phalloidin to stain exclusively F-actin, i.e. the linearly polymerized form of G-actin (globular actin), which is present only in healthy myocardium. Non-polymerized G-actin occurs when a cell's cytoskeleton has been damaged, like after MI in the infarct area, and cannot be stained with phalloidin.

In our immunofluorescence pictures, vital myocardium therefore shone in bright green (phalloidin positive), while ischemic or scar tissue was dark with low autofluorescence (phalloidin negative)[73].

Slides were mostly examined at 20-fold magnification at the Carl Zeiss Axio Imager.Z1m.

2.2.2.2. Conventional histology

Conventional histology was performed on paraffin sections that were dried overnight in the 60°C oven.

Afterwards, sections were deparaffinized in the following way:

1.	Rotihistol A	5 min
2.	Rotihistol B	5 min
3.	Xylene	5 min
4.	Xylene/ethanol (1:1)	5 min
5.	Ethanol 99 %	5 min
6.	Ethanol 75 %	5 min
7.	Ethanol 50 %	5 min
8.	Aqua dest.	dip 2-3 x

Hematoxylin and eosin (HE) stainings were done to examine heart tissue morphologically[74]. We used sections of heart tissue that were 5 µm thick and stained as described in this protocol:

1.	Hemalaun	10 min
2.	*Blue* in running tab water	10 min
3.	Aqua dest.	dip 2 x
4.	Eosin	5 min
5.	Aqua dest.	dip 2 x
6.	Aqua dest.	dip 2 x
7.	Ethanol 99 %	dip 2 x
8.	Ethanol 99 %	dip 2 x
9.	Ethanol 99 %	dip 2 x
10.	Xylene/ethanol (1:1)	5 min
11.	Xylene	5 min
12.	Rotihistol B	5 min
13.	Rotihistol A	5 min
14.	Mount with Entellan®	-

Picrosirius red (PSR) stainings were used to determine both infarct size and collagen content. Sirius red is a strong anionic dye whose sulfonic acid groups react with basic sidechains of collagen. The chemical alteration of the molecule leads to the biophysical phenomenon of enhanced birefringency, meaning a double refraction of light because of orientation-dependent differences in refractive index. In combination, staining and enhanced birefringency are specific for collagen, as published by Junqueira et al. in 1979[75].

This time, we used sections of heart tissue that were 7 µm thick. The tissue was stained in the following way:

1.	PSR solution	20 min exactly
2.	Aqua dest.	dip 2-3 x
3.	Aqua dest.	dip 2-3 x
4.	Aqua dest.	dip 2-3 x
5.	Ethanol 50 %	1-2 min
6.	Ethanol 75 %	1-2 min
7.	Ethanol 99 %	1-2 min
8.	Xylene/ethanol (1:1)	5 min
9.	Xylene	5 min
10.	Rotihistol B	5 min
11.	Rotihistol A	5 min
12.	Mount with Entellan®	-

2.2.2.3. Determination of infarct size

7 µm mid-ventricular paraffin sections of the heart were stained with PSR and used to determine infarct sizes on day 56 in a computer-assisted way. They were photographed and manually analyzed (ImageJ software version 1.44; NIH, Bethesda, USA). The epicardial and endocardial infarct ratio was separately measured by dividing epicardial (endocardial) infarct length by epicardial (endocardial) circumference. Infarct size derived from this approach was calculated as [(epicardial infarct ratio + endocardial infarct ratio)/2] x 100.

2.2.2.4. Determination of collagen content

The method of determination of collagen content in heart sections was developed in our lab by Vogel et al.[73] and is based on the finding that PSR specifically stains collagen.

At first, paraffin sections were therefore stained with PSR as described in 2.2.2.2. Conventional histology.

Under the fluorescence microscope, areas covered by vital myocardium appeared green, while the collagen in the scar area showed red fluorescence.

For all experiments, we used the same fluorescence microscope and analysis software (Zeiss Z1m, Axiovision 4.8 and ZEN 2011, data format: *.zvi). Pictures of the image section to be quantified were recorded in the following way: We used the lens with 20-fold magnification (Plan-Apochromat 20x/0.80 Ph 2 M27) and always used an exposition time of exactly 250 ms for the red (c1, rhodamine, dsred) and the green channel (c2, FITC).

Pictures were then, as far as this was possible, automatically processed: The different single channels (green and red) were extracted into JPEG format. Afterwards, those files were converted into grayscale pictures. After image subtraction and addition, the total tissue area (tissue as well as section-conditional gaps) could be calculated. The area of vital myocardium (green) or scar tissue (red) could thereby be determined.

2.2.2.5. Preparation of single-cell solutions

To obtain single splenocytes, the spleen was minced with fine scissors and strained through a 40 µm nylon mesh (Cell Strainer 40 µm Nylon, BD Falcon™, Franklin Lakes, USA). After centrifugation at 400 g for 7 min (Centrifuge 5810 R, Eppendorf, Hamburg, Germany), the pellet was resuspended with 2 ml of erylysis buffer and incubated for 2 min to deplete remaining erythrocytes. The process was stopped by filling up the tube to 50 ml with PBS. The cell solution was centrifuged again at 400 g for 7 min and the supernatant was discarded. Then, the pellet was resuspended in the remaining PBS or diluted with PBS to arrive at the required sample volume.

To extract single cells, especially lymphocytes, from the heart, the extracted tissue had to be digested to release single cells from the very rigid post-ischemic tissue containing high amounts of collagen. After macroscopical identification of scar (lighter) and vital myocardium (pink/red), we separated both parts with a scalpel and processed them individually from then on.

We digested the previously minced heart tissue with 3 ml Collagenase Type II (1000 U/ml RPMI) per sample at 37° C for 35 min in an incubator (BB 6220, Heraeus Instruments, Hanau, Germany). After digestion, heart tissue was put through a 100 µm nylon mesh (Cell Strainer 100 µm Nylon, BD Falcon™, Franklin Lakes, USA). After centrifugation, no lysis of erythrocytes was performed to nurse the few lymphocytes in the heart. However, the falcon was filled up with PBS to 50 ml and the cell solution was thoroughly poured through a 40 µm nylon mesh to get rid of any cell debris. The cleared solution then underwent a second centrifugation step. The pellet was likewise resuspended in the remaining PBS or diluted with PBS to arrive at the required sample volume.

2.2.2.6. Protein extraction

To extract proteins from tissue, it was quick-frozen in liquid nitrogen, stored at -80° C and thawed upon use. The material was then weighed (in mg) and mixed with a 3-fold volume of NaCl 0.9 % (in µl) in a 1.5 ml tube. Subsequently, the tissue was ground using a Micropistill (small pestle) for 1.5 to 2.0 ml tubes (Eppendorf, Hamburg, Germany). Tubes were centrifuged at V_{max} for 10 min, the clear supernatant transferred to a new tube and centrifuged again. The supernatant was aspirated, put on ice and analyzed for its protein concentration (in mg/ml) using NanoDrop 2000c spectrophotometer. In our studies, we used protein extracts for sodiumdodecylsulfate polyacrylamide gel electrophoresis (SDS-PAGE or Western Blot analyses and ELISA experiments respectively.

2.2.2.7. SDS-PAGE

SDS-PAGE is a moleculobiological method to separate molecules with respect to their molecular size and polarity. To make proteins or other molecules move, electricity is applied to a gel matrix in a way that molecules move towards the anode (positive pole). This is because the proteins are embedded in sodiumdodecylsulfate (SDS) which makes their face negatively charged. Physically, large proteins need a longer time to wander through the gel and can therefore be detected at the beginning rather than at the end of the gel. By adding a protein ladder (standard), the molecular weight of each molecule in a band can be exactly determined.

For our SDS-PAGE experiments, we used a Bio-Rad Mini-PROTEAN® 3 Cell system (Bio-Rad Laboratories, Hercules, USA) which was assembled in accordance with the manufacturer's information. The separation gel was prepared in a concentration of 18 %, the collection gel in a concentration of 6 %, both with a thickness of 1.0 mm.

Separation gel (18 %)	
Solution A: Acrylamide 30 %	4.5 ml
Solution B: 1,5 M Tris/HCl (pH 8.8)	5.0 ml
H_20	300 µl
SDS 10 %	100 µl
Temed	15 µl
APS 10 %	150 µl

Collection gel (6 %)	
Solution A: Acrylamide 30 %	1.5 ml
Solution D: 0,5 M Tris/HCl (pH 6.8)	2.55 ml
H_20	5.8 ml
SDS 10 %	100 µl

Temed	15 µl
APS 10 %	150 µl

At first, the separation gel was molded as far as approximately 1 cm below the edge of the glass plate and immediately covered with H_20. The gel was then rested at RT to polymerize for approximately 30 min (or until hardened). Afterwards, the water was decanted, the collection gel added and a comb (producing ten pockets) inserted. Again, the gel was left for curing (30 min). After polymerization, the gel-filled glass plates were transferred to the SDS system which was filled with SDS running buffer (0.384 M glycine, 50 mM Tris/HCl (pH 8.6), 0.1 % (w/v) SDS). The combs were removed and the pockets were checked for tightness and flushed using a buffer-filled syringe. To equally load 100 µg of protein into the pockets, the samples (in this case protein extracts) were mixed with 4-fold SDS loading buffer plus β-Mercaptoethanol in a 1:3 ratio. One pocket could comprise no more than 30 µl of sample. The gel was loaded with special tips (Gelloader Tips, no-name). 5 µl of a protein marker were filled into one pocket of each gel, preferentially at the exterior left edge (PageRuler™ Prestained Protein Ladder; Thermo Scientific, Waltham, USA). Electrophoresis was performed at 100 V for 90 - 120 min (until protein marker had almost reached the edge of the glass).

All SDS-PAGE experiments were performed to eventually be completed in a Western Blot.

2.2.2.8. Western Blot

In principle, Western Blotting allows the transfer of molecules that were separated in SDS-Page according to their molecular weight. Through the application of voltage, molecules are carried over or *blotted* to a special membrane and can afterwards be detected with antibodies. For transfer, we used the Mini Trans-Blot® Cell (Bio-Rad

Laboratories, Hercules, USA). To do so, we removed the enframed gel from the system, discarded the collection gel and incubated the remaining separation gel in ice-cold CAPS Buffer (10 mM CAPS (pH 11.0) and 10 % (v/v) methanol prepared in 1 liter of H_20). The same was done with a nitrocellulose membrane (Roti®-NC, 0.2 µm pore size, Carl Roth GmbH + Co. KG, Karlsruhe, Germany), Whatman paper and a sponge pad (all cut to gel size). The blot was then assembled (from bottom to top) in the following way: Clear bottom – sponge pad – Whatman paper – NC membrane – gel – Whatman paper – sponge pad – dark top. To remove air bubbles in the *sandwich* a small roller was used to smooth down the Whatman paper. The blot carrier was closed and conveyed to the blotting system to which we applied a voltage of 50 V (180 mA) for 60 min. During the blotting process, the system was filled with CAPS Buffer (see above), internally cooled with a cooling element and externally cooled with ice.

After blotting, the membrane was transferred to H_20 and afterwards stained with Ponceau S solution (0,25 % (w/v) Ponceau S in 1 % (v/v) acetic acid). After washing it briefly with H_20, the membrane was examined to assess equal loading of pockets (temporary loading control) and scanned using a commercial flatbed scanner. The membrane was then incubated in TBST (150 mM NaCl, 10 mM Tris/HCl (pH 7.4), 0.1 % (w/v) Tween-20) containing 5 % (w/v) of nonfat dry milk at RT for one hour to prevent unspecific binding of the antibody.

Afterwards, the primary antibody was applied in a concentration of 0.1 µg/µl (2,5 µl of anti-CXCL13 Ab in 5 ml of TBST – 5 % milk) and the membrane was incubated under constant agitation overnight at 4 °C. When possible, the membrane was shrink-wrapped to save antibody. The next morning, the membrane was washed in TBST (3 x 7 min) and incubated with the secondary antibody in a dilution of 1:5000 (anti-goat IgG rabbit pAb linked to HRP) for 30 min. The membrane was then washed again (see above). All incubation and washing steps were carried out on a shaker.

Next, the membrane was covered with ECL (1 ml of solution A + 1 ml of Solution B) using a commercial kit (Amersham™ ECL™ Prime Western Blotting Detection Reagent) and immediately scanned at the LI-COR Scanner at high sensitivity detection level.

To use the same membrane for the detection of another antigen, the membrane had to be stripped, i.e. cleared of all remaining antibodies, before immunofluorescence staining could be repeated. For that reason, we incubated the membrane for 30 min with a self-mixed mild strip buffer (15 g glycerine, 1 g SDS, 10 ml tween; pH 2,2) and afterwards washed it with Aqua dest. and 1 x 7 min with TBST. Hereafter, a new staining (e.g. for a loading control) could be performed.

2.2.2.9. ELISA

ELISA (enzyme linked immunosorbent assay) is a technique in which a soluble antigen (in this case: CXCL13), e.g. in serum or in our case in a protein extract (50 µl), produced as described in 2.2.2.6. Protein extraction, can be detected using a solid phase (well on a plate) pre-coated with a specific so-called capture antibody (in this case: anti-CXCL13). After antigen-antibody-binding, a detection antibody linked to horseradish peroxidase (HRP) is added. In presence of hydrogen peroxide (a donator of protons), HRP can reduce a dye molecule (in our case: not specified, only referred to as "substrate solution") and thereby provokes a color change which can be quantified. Establishing a calibration curve by measuring the light emission of a dilution series and known samples allows for exact determination of the concentration of the antigen – as expressed in Lambert-Beer's rule – in each sample.

$$\boldsymbol{E = e \cdot c \cdot d}$$

E Extinction

e molar extinction coefficient (cm^2/mol)

c concentration of a substance (mol/cm^3)

d thickness of the cuvette (cm)

In our experiments, we used a commercial ELISA kit for CXCL13, the Mouse CXCL13/BLC/BCA-1 Quantikine ELISA Kit by R&D Systems (Minneapolis, USA) and carried out the assay respecting the manufacturer's instructions. The signal strength of each well was determined with a photometer (Dynex MRX^{e} tc; Magellan Biosciences, North Billerica, USA) and visualized and analyzed using GraphPad Prism 6 (Statcon, Witzenhausen, Germany).

2.2.2.10. Flow cytometry (FACS)

FACS (fluorescence activated cell sorting) is an immunological method to examine single cell solutions or samples according to cell surface markers. Analysis is very accurate, flexible and allows a high throughput of cells. In this context, we refer to FACS as mere flow cytometry without subsequent sorting of the stained cells. This process is referred to as FACS Sort and described in 2.2.2.11. Cell sorting (FACS sort).

For all our flow cytometry experiments, we used a FACS Canto II (Becton Dickinson, Heidelberg, Germany) which consists of three lasers – a blue (488 nm), red (633 nm) and violet (405 nm) one – and eight fluorescence detection channels.

In principle, cells or particles (e.g. compensation beads) are stained with fluorescent dyes linked to antibodies against specific epitopes on the cell surface (e.g. clusters of differentiation, CD). In the measuring chamber, the so-called nozzle (A), the sucked-in single cell suspension is accelerated within a laminar sheath flow and spread out to an – ideally – one-cell wide stream (B). This is crucial to analyze truly single cells and not doublets, triplets or dirt particles. The analyzing laser excites the single cells with a certain wave length which produces the following data sets for each cell (C):

- FSC (forward scatter): Originates from deflection at the cell's surface and is measured at 175° relative to the laser beam, it is a measure of cell size (X axis).

- SSC (side scatter): Is caused by refraction/aberration of light at subcellular structures and is determined at 90° relative to the laser beam, it is a reading of cell granularity (Y axis).

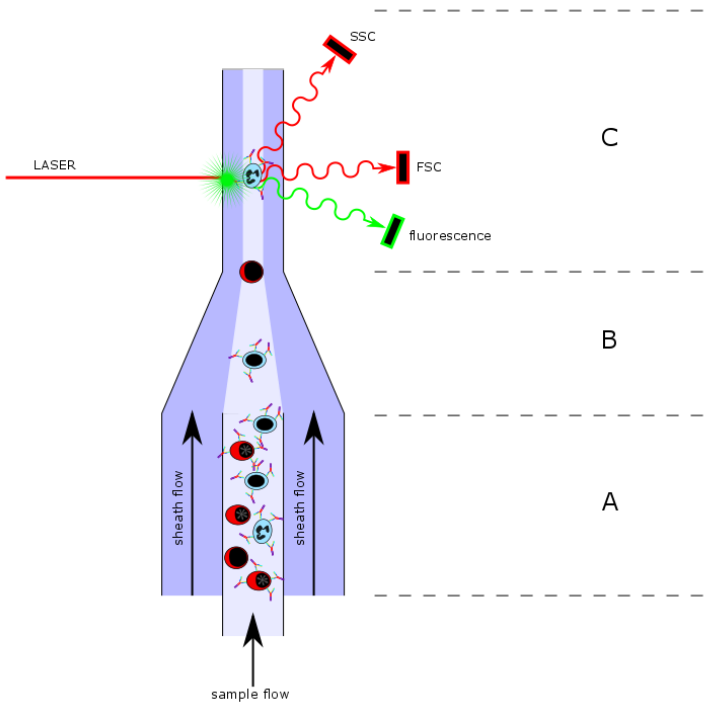

Figure 3: Single cells are excited by the laser and analyzed according to their FSC (cell size) and SSC (granularity) as well as their specific fluorescence.

FSC and SSC can always be measured, even using unstained cells, as it is determined independently from any fluorophores and just referring to the physical features of a cell.

In a pre-analysis during measuring, cells that are strikingly different from the targeted cell population can be excluded right from the beginning. This might be because their FSC is too high, indicating that these cells might be too large and are suspected to be doublets etc. or because their granularity is too high, indicating that the bits measured are dirt particles. Thus, pre-selection of cells through a FSC-SSC plot is possible and even essential.

The third parameter determined in the measuring chamber is the cell-emitted fluorescence. After excitation, fluorophores absorb a certain amount of light and then emit light of another wave length. Afterwards, this fluorescence spectrum is split up by a dichroic filter and an interference filter into the spectral ranges typical for each color. Multiple fluorophores on one cell can therefore be analyzed simultaneously.

However, if several dyes are used simultaneously, compensation is necessary because the spectra of some colors overlap. Therefore, single stainings must be performed before each experiment to obtain data which, typed into a software system, can be used to detect such redundancies and mathematically correct them.

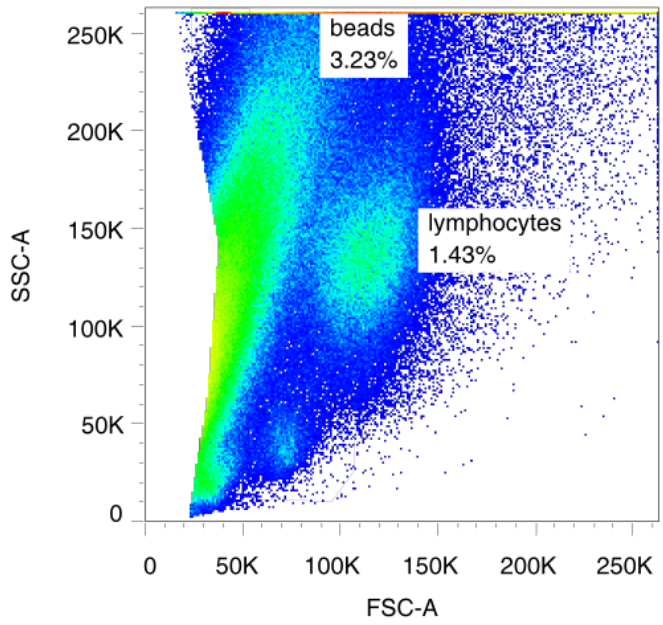

Figure 4: Typical FACS plot (FSC-A/SSC-A) showing lymphocytes and counting beads.

Sample preparation:

Samples were prepared as described in 2.2.2.5. Preparation of single-cell solutions to produce single cell solutions out of murine heart or spleen.

Surface staining:

Afterwards, the cell suspensions were stained in sterile, U-bottom 96-well plates (Cellstar®; greiner bio-1, Greiner, Frickenhausen, Germany). We used 10^6 cells per well (spleen) and 200 µl of blood and heart sample respectively (assuming they might contain a maximum of 10^6 cells). When exact cell numbers were needed, we calculated them using a commercial cell counter (TC10™ Automated Cell Counter; Bio-Rad Laboratories, Hercules, USA) as described in the manufacturer's protocol. We measured samples diluted in Trypan Blue Solution (0.4 %) purchased from Sigma-Aldrich Chemie (Steinheim, Germany): For the heart samples, we mixed 1 µl of sample with 9 µl of Trypan Blue; for the spleen samples, we pre-diluted samples 1:100 and equally mixed 1 µl of this solution with 9 µl of Trypan Blue. The sample-filled plate was centrifuged at 400 g for 7 min and the supernatant was discarded. The pellet was resuspended with 25µl of F_c blocking antibody (Anti-CD16/32, TruStain fcX™; BioLegend, San Diego, USA) in PBS in a concentration of 0.5 mg/ml diluted 1:500 and incubated for 15 min at 4°C. Subsequently, FACS antibodies were added in 25 µl PBS to each well (0,5 µl antibody/target), the sample was gently mixed and incubated for 30 min at 4 °C. Then, wells were filled up to 200 µl with PBS (washing step), centrifuged (at 400 g for 7 min) and pellets resuspended with 200 µl of PBS (used as FACS Buffer). We always additionally analyzed a non-stained sample as a negative control in addition to single stainings for each antibody.

Compensation/single stainings:

We either performed single stainings with target cells in single-cell suspension or used compensation beads (anti-rat and anti-hamster Ig, κ; BD Biosciences, Franklin Lakes, USA), which are polystyrene microspheres that are either coated with IgG (positive compensation beads) reacting with all mouse or rat/hamster isotypes or uncoated (negative compensation beads). Upon addition of a fluorescent antibody, those particles can also be stained and used as positive and negative controls. We used the compensation beads as described in the manufacturer's protocol, mostly to save cells.

As beads are artificial, they have no autofluorescence. To rule that out, one real sample remaining unstained is always necessary.

Cell counting:

In most experiments, it was necessary to have an absolute cell count to calculate cell frequencies. To count cells, we used counting beads (CountBright™ Absolute Counting Beads; Invitrogen, Carlsbad, USA) in the flow cytometer (FACS Canto II; Becton Dickinson, Heidelberg, Germany). A defined volume of the bead suspension (here: 50 µl) is added to each sample. The CountBright™ suspension contains a specific number of beads/50 µl (variable C) determined by the specific bead lot number. As stated by the vendor, the beads are excited by all lasers emitting light from UV to 635 nm and fluoresce brightly in all channels between 385 nm to 800 nm. By comparing the ratio of beads events (usually 10,000 events in the bead gate) to cell events (without debris and dead cells) it is possible to calculate absolute cell counts in the sample.

$$\boldsymbol{concentration\ of\ sample}\ [\boldsymbol{cells}/(\mu\boldsymbol{l})]\ = \frac{\boldsymbol{A}}{\boldsymbol{B}} * \frac{\boldsymbol{C}}{\boldsymbol{D}}$$

A number of live target cells

B fixed number of beads counted in the flow cytometer (10,000 beads)

C number of counting beads in 50 µl/in sample according to bead lot number

D final volume of sample (in µl)

Fixation/storage of cells:

Because we could not always analyze cells immediately after sample preparation, they had to be stored. If storage lasted less than 12 hours, we kept the cells resuspended in

PBS (see above) at 4° C in a dark environment (refrigerator) and mixed wells thoroughly again prior to measuring. If storage lasted more than 12 hours, we fixated the cells with formalin (4 % formaldehyde in PBS), i.e. we resuspended cells in 100 µl of PBS and 100 µl of formalin instead of 200 µl of PBS (finally resulting in a 2 % formaldehyde concentration) and subsequently stored them at 4 °C. Formaldehyde denatures proteins and thereby stabilizes antigen-antibody-interconnections. However, fixation also alters FSC and SSC requiring an adjustment of voltages. Fixation of cells also impedes comparisons with experiments with non-fixated cells. In some cases, heart samples were altered to a degree that made it impossible to correctly analyze them. We therefore decided not to fixate cells whenever possible.

Gating strategy for target cells:

If we stained lymphocytes – as in most cases – we gated conforming to the following strategy: After compensation by means of single stainings, we determined a *life gate* in the FSC-SSC plot to exclude dead cells, dirt and small particles (FSC threshold: 5,000). After spotting vivid lymphocytes ($CD45^+$), we gated for other surface markers such as $B220^+$ for the B cell population. The combination of several markers is, in most cases, specific for a certain cell type or subpopulation.

2.2.2.11. Cell sorting (FACS sort)

In our experiments, we performed several cell sorting assays. In principle, FACS sort works just like flow cytometry with the special feature that cells are not only marked and measured but can also be collected depending on their surface marker profile. It is therefore possible to sort out distinct cell populations or subsets. We used this method to selectively sort B cells and monocytic cells from heart tissue and spleen. In detail, we extracted the desired organs as described in

2.2.1.5. Harvesting of organs and washed them in RPMI solution before flushing them with digestion buffer - Collagenase Type II (360 U/mg) in RPMI in a concentration of 3

mg/ml (≈ 1000 U/ml). Afterwards, we minced the organs with fine scissors on a glass plate and digested them with 3 ml of digestion buffer per sample at 37 °C for 35 min in 4.5 ml FACS tubes in an incubator (BB 6220, Heraeus Instruments, Hanau, Germany). Subsequently, we put the samples through a 100 µm nylon mesh (Cell Strainer 100 µm Nylon, BD Falcon™, Franklin Lakes, USA) with the help of a pestle. Cells were then transferred to 15 ml tubes which were filled up with BSS/BSA. After centrifugation (7 min at 515 g), the supernatant was discarded. Meanwhile, we diluted 2.2 ml of FCS with 40 ml of RPMI and resuspended each pellet in 175 µl of that solution. Next, we added an F_c blocking antibody (TruStain fcX™/anti-CD16/32; BioLegend, San Diego, USA) in 25 µl of PBS in a concentration of 0.5 mg/ml (diluted 1:500) and incubated it for 15 min at 4 °C in a dark environment. Afterwards, cells were stained by directly pipetting the respective antibodies into the solution (concentration: 1:100 → 2 µl or 1:50 → 4 µl in samples containing a myriad of cells) and incubated for 15 min at 4 °C. Another centrifugation step followed, the supernatant was discarded and the cells were resuspended with 500 µl of the FCS-RPMI solution. The sample was then directly grinded through a 4.5 ml FACS tube with cell-strainer cap of 40 µm pore size (BD Falcon™; BD Biosciences, Franklin Lakes, USA) and another 150 µl (or 500 µl with high-cell-amount samples) of FCS in RPMI added. The samples were stored on ice until sorting was performed.

After sorting, the cells were collected in 340 µl of RLT buffer (taken from the RNeasy Mini; Qiagen, Hilden, Germany) mixed with 10 µl of ß-Mercaptoethanol in 1.5 ml biopure tubes (sterile etc.), immediately frozen in liquid nitrogen and stored at -80 °C.

2.2.2.12. RNA Amplification

In several experiments, initial RNA amounts were too low to use in real time (RT-)PCR experiments after extraction from e.g. sorted B cells with the RNeasy Micro Kit. Therefore, we amplified RNA whenever this was necessary with the C&E Version

ExpressArt mRNA amplification Pico kit (AmpTec GmbH, Hamburg, Germany) as reported by the manufacturer's instruction manual. The procedure is based on the principle of PCR amplification in three amplification rounds transcribing RNA first into cDNA and then back into RNA. This procedure is repeated three times and includes purification steps on columns after each transcription. Unfortunately, exact details cannot be mentioned because the manufacturer does not reveal them.

After three amplification rounds, we checked the augmented RNA amount measuring each sample's concentration using NanoDrop 2000c (Thermo Scientific, Waltham, USA). For all our RT-PCR experiments we used 1 µg of RNA, digested it first with DNase (DNase 1 Amplification Grade; Sigma-Aldrich Chemie, Steinheim, Germany) and then transcribed it into cDNA using a cDNA Synthesis Kit (iScript™ cDNA Synthesis Kit; Bio-Rad Laboratories, Hercules, USA).

In general, amplified samples did not show any abnormalities in experimental read-outs or in results when compared to non-amplified samples.

2.2.2.13. RT-PCR

RT-PCR is a technique that can be used to detect and quantify gene expression in cDNA out of RNA (total or mRNA only) extracted from total tissue or from single cells (cell culture/FACS-Sort). Basically, RT-PCR works just like a regular PCR (polymerase chain reaction), in which prior to the experiment RNA is transcribed into cDNA and then replicated a certain number of times using probes/primers (two primers that are complementary to the 3' ends of each of the sense and anti-sense strand of the DNA target) specific for a certain gene (e.g. Cxcl13 for CXCL13). We usually had samples undergo 40 cycles of amplification. Before the reaction, the plate is preheated to 50 °C for 2 min and afterwards to 95 °C for 10 min.

The term *real time* (RT) refers to the possibility to watch the reaction in progress or live, i.e. in real time due to an attached computational device depicting curves for all the samples. PCR results not in a linear amplification of nucleic acids but in an exponential augmentation $2^{number\ of\ cycles}$. Under ideal experimental conditions, with every cycle, the number of target molecules doubles resulting in an efficiency $E = 1.0$. Under realistic conditions however, efficiencies between 0.8 and 0.9 are achieved. Efficiency should be tested in each experiment to assess the value of a result.

Probes in our experiments were purchased from Life Technologies (Darmstadt, Germany) and were tagged with the fluorophore 6-FAM-phosphoramidit at the 5' end of the probe. The excitation wavelength of FAM is 488 nm; emission is at 518 nm. The 3' end of the probe is associated with a so-called quencher. Without enzymatic activity, the quencher suppresses the reporter function of the dye. Upon exposition with the Taq polymerase – as in PCR reaction – the dye is however cut from the probe by the enzyme's 5' exonuclease activity and its emitted fluorescence can be determined. The signal intensity of the fluorescent reporter probe is therefore a direct measure (quantification) of the gene expression, i.e. the amount of mRNA-specific cDNA which is amplified. The higher the signal we detected, the higher the specific gene expression was.

In PCR reactions, there are mainly three steps:

- **Denaturation:** Heating of cDNA sample to 95 °C to cause DNA melting and thereby produce single-strand DNA molecules (15 s)
- **Annealing:** At 60 °C, primers can bind to the single-stranded DNA template; afterwards, the Taq polymerase begins complementary DNA synthesis
- **Elongation:** The Taq polymerase continues to synthesize DNA in a speed of roughly 1000 bases per second; in an ideal set-up, at each extension step, the amount of DNA target is doubled
- **Final elongation:** Performed for 5 – 15 minutes after the last amplification step to fully amplify all remaining single-strand DNA molecules
- **Final hold:** For short-term storage after the reaction (at 15 °C)

In all our experiments, we used GAPDH as a housekeeping gene, which is a gene that presumably has a stable expression level in different kinds of tissues even under changing conditions (e.g. hypoxia). In some experiments, we used a second or third housekeeping gene (e.g. Actb) to make sure the results were indeed valuable. For each gene, the threshold was individually calculated, mostly using the auto calculation option in the iCycler software (Bio-Rad Laboratories, Hercules, USA). If the threshold could not automatically be placed within the region of linear slope of the curves, it was corrected manually. The expression value for each gene in each well was calculated using $f = 2^{-\Delta CT}$ for an ideal efficiency of $E = 1.0$ and using $f = (1+E)^{-\Delta CT}$ for other efficiencies. Afterwards, the expression level of each gene was visualized in a bar graph.

2.2.3. Statistical Analyses

All statistical data analyses were performed with GraphPad Prism 6.

If not otherwise stated, results are presented as mean±SEM per group. For comparisons of two groups, we used an unpaired t- test.

For multiple comparisons, we performed a one-way ANOVA statistical test. Survival data is shown as Kaplan-Meier curves, and data was analyzed by a log-rank test. Differences were considered significant at $p < 0.05$ (*), very significant at $p < 0.01$ (**) and highly significant at $p < 0.001$ (***).

3. Results

3.1. Infiltration kinetics and localization of B cells after MI

This project started from the observation that B cells are present in the murine heart following experimental myocardial infarction. Although some B cells occur also in the healthy heart under physiological conditions, we were interested in possible post-MI alterations, e.g. regarding cell count and function.

From earlier studies, we knew that lymphocytes, especially activated T cells, can be detected in heart-draining lymph nodes as well as in the infarcted myocardium[66]. Although little was known about B cells at the time, we reasoned that they might similarly play a decisive role.

Our first aim was to find out how many B cells exactly populated the myocardium after infarction, at which time point they peaked and where exactly they were localized. Therefore, we produced frozen sections of murine hearts on day one, three, seven, 14 and 56 post MI, stained them and afterwards analyzed them planimetrically with a fluorescence microscope.

To distinguish between infarct area/scar and unaffected tissue in our immunofluorescence pictures, we used phalloidin to stain vital myocardium, shining bright green (phalloidin positive), while ischemic or scar tissue is dark with low autofluorescence (phalloidin negative). See also 2.2.2.1. Histology and immunofluorescence microscopy.

To stain B cells, we used a fluorescent antibody against B220 detectable in the blue (Cy5) channel (Figure 5). In mice, unlike in humans, B220 (a CD45 isoform and member of the T200 glycoprotein family) is a pan B-cell marker as discovered in 1981[76]. We correlated the number of B cells (double positive for B220 and DAPI) within the field of view in the

fluorescence microscope with the area of their localization. We thereby differentiated three different areas: Scar (infarct area), septum (vital myocardium) and border zone (transition zone). We were especially interested in the phalloidin negative region, i.e. the infarct area, and the border zone (Figure 5). The so-called septum region (non-infarcted myocardium) served as a reference as the infarct zone was widely confined to the left-ventricular free wall.

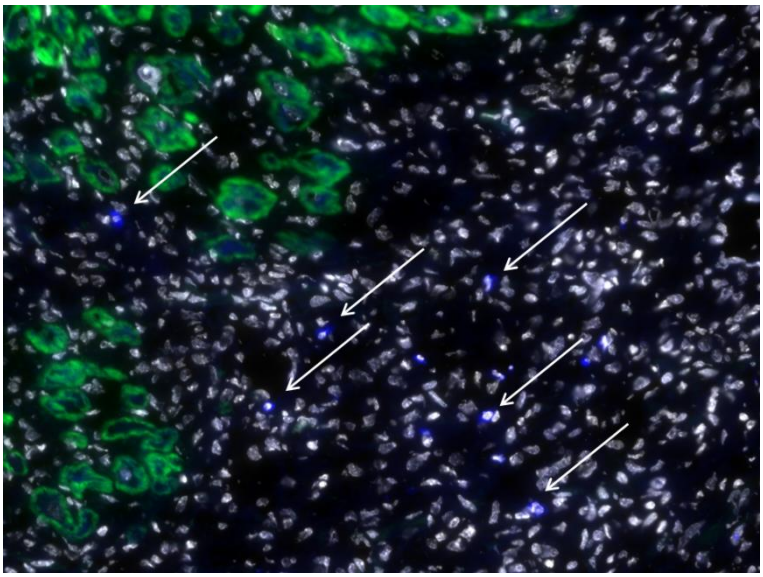

Figure 5: B cells (arrows) are positive for B220 (blue) as well as DAPI (white) and localize in the border zone of the infarct area (phalloidin negative = dark) and vital cardiomyocytes (phalloidin positive = green); day 7 after myocardial infarction.

We then analyzed all the photographs using a method developed in our laboratory. We took pictures with the camera of our fluorescence microscope in the following way: First, we selected an area in the border zone microscopically depicting equal parts of scar (dark) and vital tissue (green). Starting from there, we then scanned through the respective section five fields of view (in the following referred to as *squares*) vertically (to the top and to the bottom of the section) and horizontally in both directions towards scar and septum. For more details, see Figure 6.

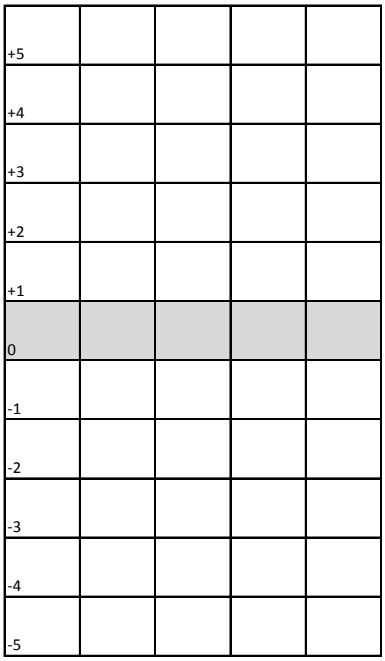

Figure 6: Planimetrical evaluation of relative B-cell numbers per mm^2 heart tissue with a fluorescence microscope starting from the left square in row 0.

We used the same fluorescence microscope and analysis software (Zeiss Z1m, Axiovision 4.8 and ZEN 2011, data format: *.zvi) for all experiments. We used the lens with 20-fold magnification (Plan-Apochromat 20x/0.80 Ph 2 M27) and always set an exposition time of exactly 3000 ms for the blue channel (Cy5) and 12 ms for the DAPI channel. For the green channel (FITC), we had to define the exposition time individually in each experiment because the color intensity was always slightly different. It was mostly between 54 and 132 ms.

All pictures were then analyzed with ZEN 2011 (blue version). We manually circuited the phalloidin positive (green) area in each picture and then assessed the phalloidin negative area by subtracting the phalloidin positive area from the total area of the picture. We finally received a value in µm for each area. Subsequently, we counted the B cells (double positive for B220 and DAPI) in both areas and calculated the relative B-cell count per mm^2 of intact myocardium or scar tissue.

We repeated this experiment with n = 2 - 4 MI and n = 1 sham animals on day one, three, seven, 14 and 56. We found that B-cell frequencies in intact myocardium (phalloidin positive) did not change significantly over time. We could, nevertheless, detect some B cells also in sham-operated mice (7.85 cells/mm^2 on average).

Interestingly, we could indeed show that the number of B cells was rising in the infarcted (phalloidin negative) region of the heart over time. On day one, there were 35.17 B cells/mm^2. The B-cell influx peaked on day seven with a mean value of 45.41 cells/mm^2. Afterwards, the numbers gradually declined until day 56 (see Figure 7).

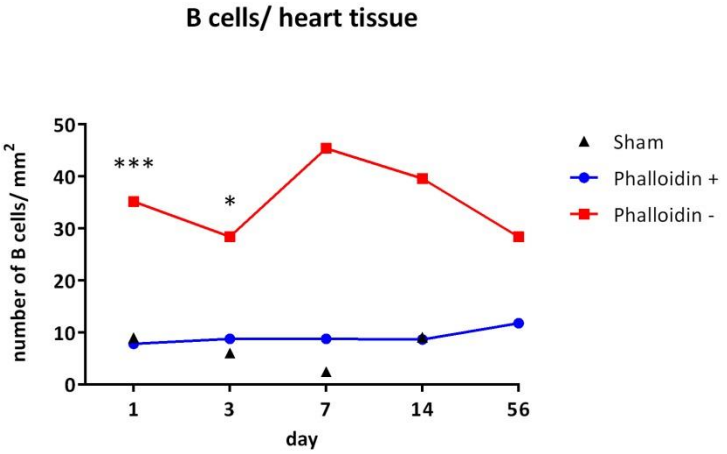

Figure 7: B cells can be found in infarcted (phalloidin negative) areas of the heart after myocardial infarction peaking on day 7. Numbers are significantly higher in phalloidin negative than in phalloidin positive areas on days 1 (***) and 3 (*). In sham-operated animals, there are only few B cells.

When we compared B-cell frequencies in sham-operated animals with those in the septum (vital myocardium) of operated (MI) animals over time, we saw that they were not much of a difference. That suggests that it must be some factor exclusively present in the infarct area that is responsible for the attraction of B cells (see also 3.3. The chemokine CXCL13 and its role in myocardial infarction)

3.2. Characterization of the B cells infiltrating the myocardium

Next, we wanted to find out what kind of B cells infiltrated the myocardium after myocardial infarction and what function they exerted there.

We therefore harvested hearts from mice three and seven days after infarction, macroscopically identified the area of infarction (usually appearing much paler than vital heart tissue), and separated it from the septum. We then processed the tissue samples into single-cell suspensions (see 2.2.2.5. Preparation of single-cell solutions). Afterwards, we performed FACS analyses by using specific FACS antibodies against certain surface antigens (see 2.2.2.10. Flow cytometry (FACS)) to differentiate between the various B-cell subsets. During analysis, we gated according to two different gating strategies.

With a combination of these stainings, we could differentiate between certain B-cell subsets:

CD5	B1 B cells: $B220^+$, $CD5^+$
IgD	Mature B cells: IgD^+, IgM^+
IgM	Progenitor B cells: IgD^-, IgM^-; Immature B cells: IgD^-, IgM^+
CD138	Plasma cells: $B220^-$, $CD138^+$
CD21	Marginal zone B cells: $CD23^-$, $CD21^+$
CD23	Follicular B cells: $CD23^+$, $CD21^+$

Firstly, we gated for $CD45^+$ cells, which are lymphocytes in general. Out of those, we determined B cells by plotting B220 against CD45. B cells are positive for both markers. Mature B cells are, in contrast to their immature precursors, highly positive for IgD and IgM. Plasma cells, which could only scarcely be found, are positive for B220 and CD138 (Figure 8).

Secondly, we looked for marginal zone B cells ($CD21^+$, $CD23^-$) and follicular B cells ($CD21^+$, $CD23^+$), originally known for instructing adaptive immune responses in the spleen. It has been known for a certain time that especially marginal zone B cells sometimes also exert innate immune functions such as supporting fast antibody responses in a T-cell-dependent and T-cell-independent way[77]. Finally, it is conceivable that de-novo formation of lymph follicles might also occur in extra-lymphatic tissues such as the heart, as described in other organs already[78]. In our earlier histological studies (s.o.) we were, however, not able to detect any.

We also checked for B1 B cells. It is common belief that B1 and B2 cells exist in mice, while in humans this concept is still topic of discussion[79]. B1 B cells belong to the innate immune system and produce mostly natural antibodies such as IgM and IgA. It is possible to discriminate between $CD5^-$ and $CD5^+$ B1 B cells[80]. The latter cells produce natural IgM and were therefore in our field of interest, they are also $B220^+$ (Figure 9).

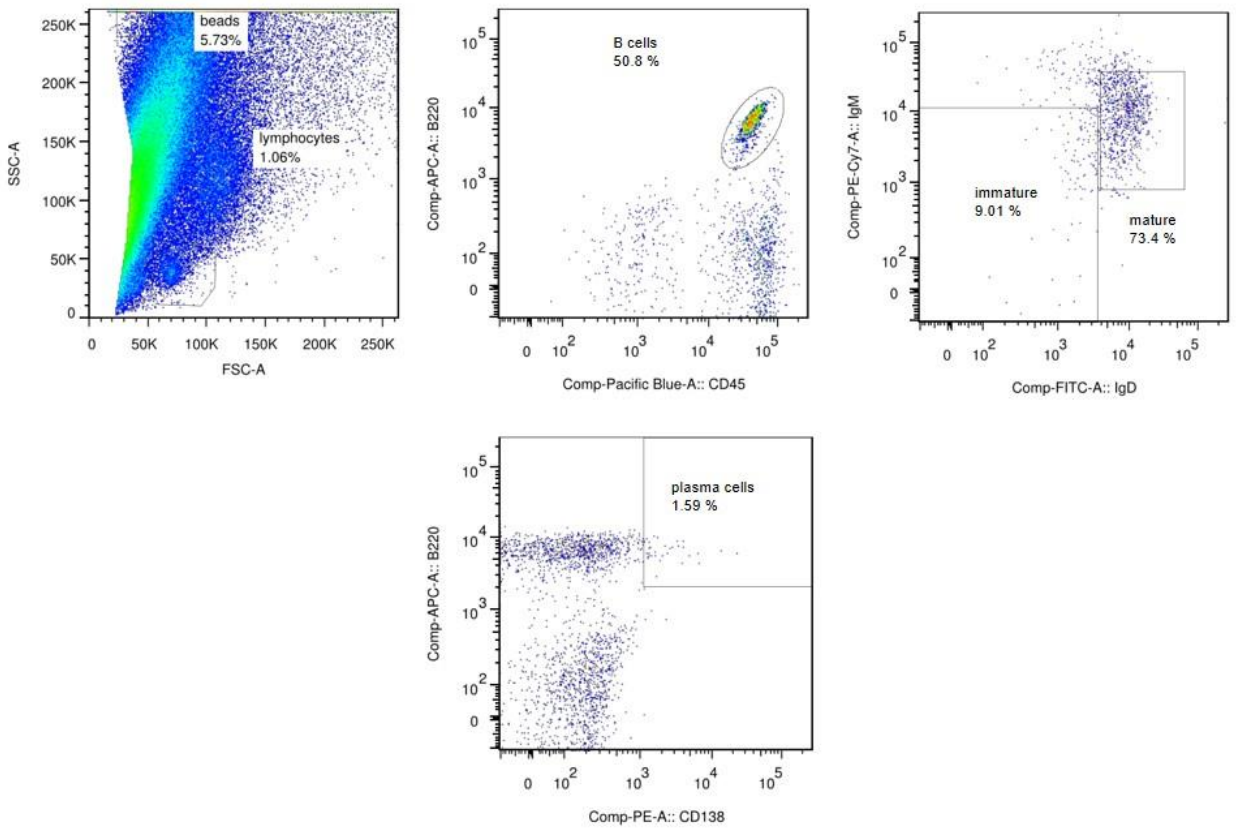

Figure 8: Gating strategy I to differentiate immature and mature B cells as well as plasma cells to be exemplary for scar tissue.

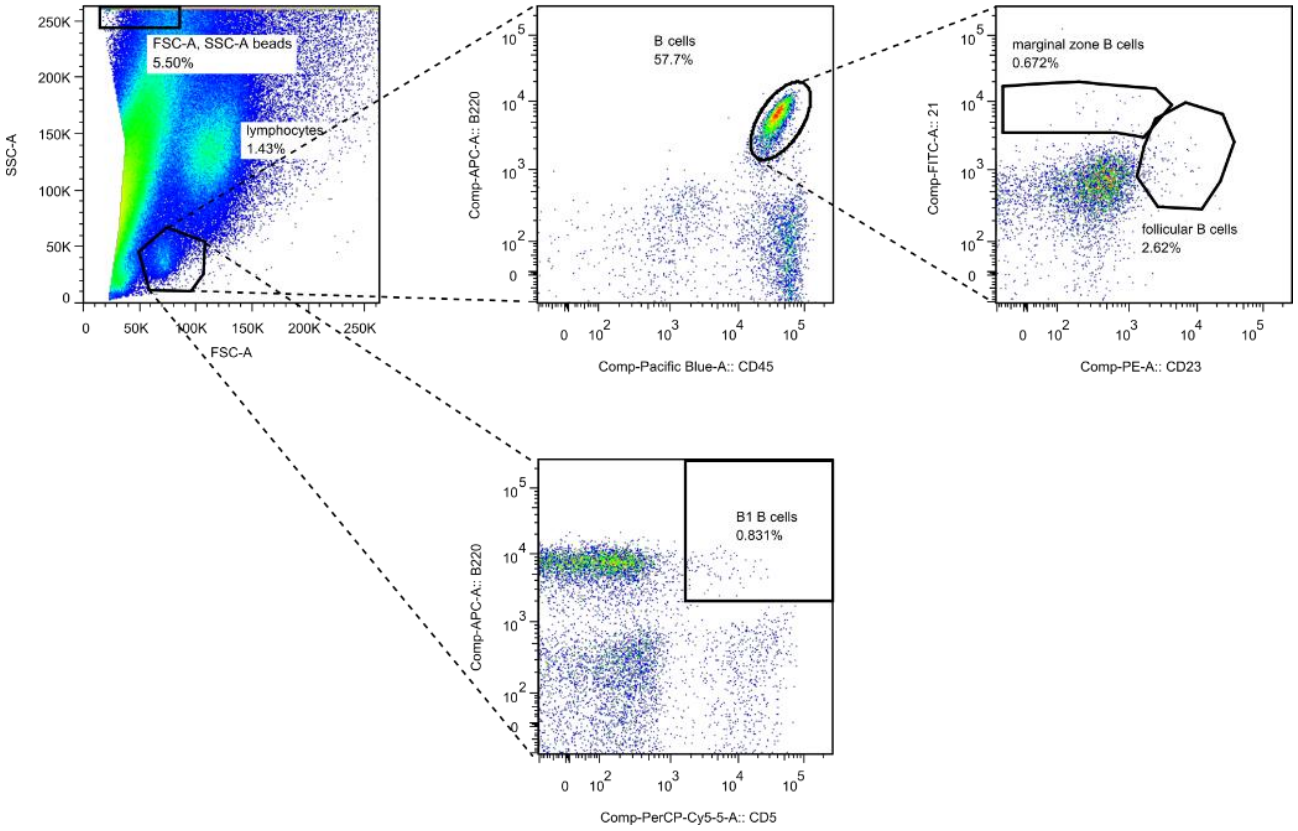

Figure 9: Gating strategy II to differentiate marginal zone and follicular B cells as well as B1 B cells to be exemplary for scar tissue.

During all our measurements, we used counting beads (see also 2.2.2.10. Flow cytometry (FACS)) to assess the exact number of cells for each group. Afterwards, we could correlate the absolute cells count with the weight of the invested heart tissue (in mg).

We found that after myocardial infarction, most B cells in the heart are mature B cells (67.8 %). Plasma-cell numbers were vanishingly low (1.0 %). There were 0.8 % B1 B cells. Marginal zone (0.6 %) and follicular (2.6 %) could only scarcely be found. Or at least that is what it seemed like. However, when we examined the plotting of CD23 against CD21 in Figure 9 closely, we saw that there was no distinct $CD23^{+}$ or $CD23^{high}$ cell population. Strictly speaking, that is why we could not distinguish follicular B cells ($CD21^{+}$, $CD23^{+}$).

We assumed that the collagenase II used to digest the heart also affects the CD23 surface antigen and cleaves it so that it cannot be detected by the respective anti-CD23 FACS antibody anymore (see also 2.2.2.5. Preparation of single-cell solutions).

This theory was supported by findings in the spleen. FACS analysis of naive, undigested spleen revealed a distinct $CD23^+$ cell population, presumably follicular B cells (Figure 10, left). In analysis of previously (with collagenase II) digested tissue, however, no such population was detected. There was only a conglomeration of cells that were far less positive for CD23 (Figure 10, right).

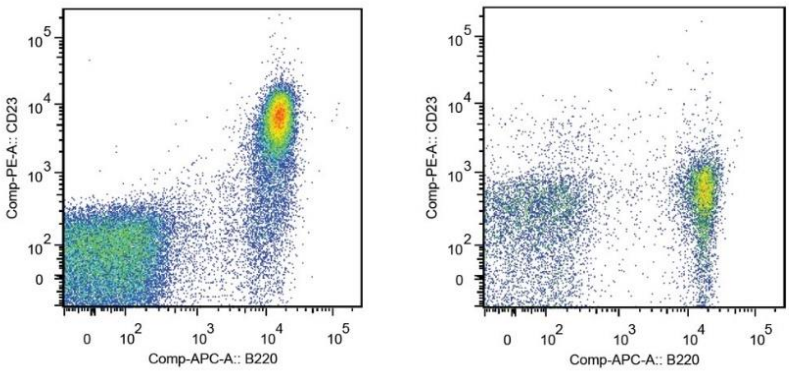

Figure 10: FACS analysis of native spleen (left) and spleen digested with collagenase II (right); digestion with collagenase II apparently leads to the disappearance of a distinct $CD23^+$ cell population.

Because of this obstacle, we tested alternative tissue digestion protocols including collagenase I (450 U ml^{-1}), collagenase XI (125U ml^{-1}), DNase I (60 U ml^{-1}), and hyaluronidase (60 U ml^{-1})[56]. None of them worked properly enough to release single cells from the collagenous and very tenacious scar tissue for a FACS analysis. We also tried another anti-CD23 antibody but unfortunately it did not work either.

Therefore, we finally did not persevere with the idea of providing information on $CD23^+$ follicular B cells anymore.

In conclusion, we can say that most of the B cells infiltrating the myocardium after infarction are apparently mature B cells, putatively experiencing T-cell dependent and independent activation and recognizing antigens via their BCR. Follicular B cells are in most cases activated independently of T cells, whereas B cells and B1 B cells preferentially undergo T cell-independent activation[80]. All of them are mature B cells.

Furthermore, B cell activation is amplified via CD21, if existent (like in follicular and marginal zone B cells). When a B cell recognizes an antigen via its BCR, CD21 simultaneously binds complement C3 if the antigen is tagged therewith. This leads – via CD19 and CD81 – to a reduced threshold for the activation of the cell[81].

Mature B cells in the context of myocardial infarction might produce natural antibodies like IgM or IgA.

3.3. The chemokine CXCL13 and its role in myocardial infarction

CXCL13 or BLC (B lymphocyte chemoattractant) is a small protein (12 kDa in mice) encoded by the Cxcl13 gene and belonging to the CXC chemokine family.

Under physiological conditions, CXCL13 is a key mediator of lymphocyte trafficking in secondary lymphatic organs, namely the spleen, lymph nodes as well as lymphoid follicles in MALT (mucosa-associated lymphoid tissue) organs.

A role of CXCL13 and/or its receptor CXCR5 (BLR1) in B-cell recruitment to the site of inflammation or disease could up to this point be demonstrated in atherosclerosis[82], neuroinflammation[83] and multiple sclerosis[84], connective tissue diseases like Sjögren's syndrome[85] and rheumatoid arthritis[86]. In some of these diseases, elevated CXCL13 and/or CXCR5 levels were observed even without the morphological correlate of lymph follicles. We therefore identified CXCL13 and its receptor CXCR5 as a potential candidate

mediating B-cell recruitment into the damaged myocardium. Besides, we also took CXCL12 ↔ CXCR4[87] and CCL19 ↔ CCR7[88] as alternative and well-known B-cell chemoattractants into consideration.

3.3.1. CXCL13 is localized next to B cells in infarcted areas

To evaluate whether CXCL13 can be found within the myocardial lesion, we examined histological heart sections on day three after MI with a fluorescence microscope. Again, we stained the vital myocardium with phalloidin and B cells with an anti-B220 antibody (see 2.2.2.1. Histology and immunofluorescence microscopy and 3.1. Infiltration kinetics and localization of B cells after MI). To stain intracellular CXCL13, we used an anti-CXCL13 antibody. Additionally, we added DAPI to mark cell nuclei.

Before we tried the staining on heart tissue, we established the method on splenic sections where CXCL13 is reported to be found in between the densely packed cells – above all B cells – forming a lymph follicle (Figure 11).

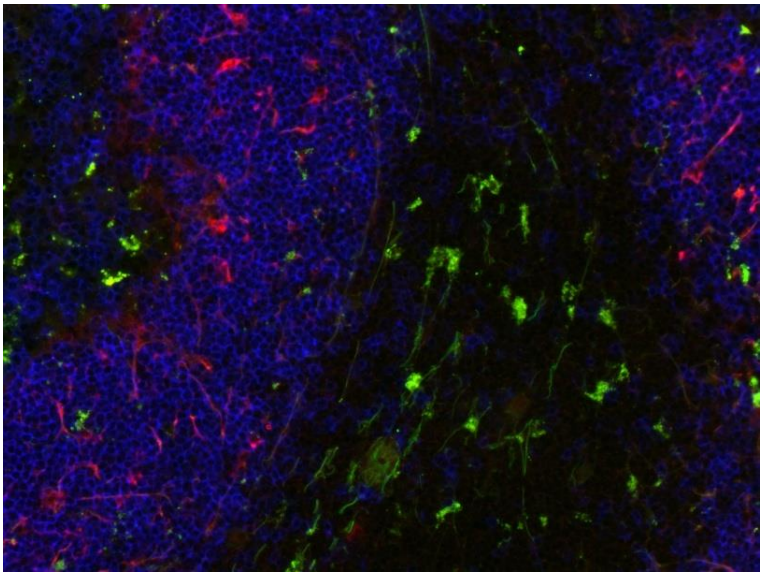

Figure 11: CXCL13 (red) in the spleen, in thread-like formations within lymph follicles that are rich of $B220^+$ B cells (blue). The splenic tissue in between the follicles shows, in spots, a relatively strong autofluorescence (green).

In our heart sections, we could – as described earlier – spot several B cells ($B220^+$, $DAPI^+$) in the scar region and border zone. Next to these, we detected $CXCL13^+$ positive cells (Figure 12), some of which seem to be clustered around areas rich of B cells in the scar. Because we evaluated day three after myocardial infarction, we expected there to be far more B cells than naturally occur in the heart under physiological conditions. To verify this, we also stained the so-called septum, the vital myocardium at the opposite of the infarct area. We could only find some rare and discretely distributed B cells (Figure 13). Other than that, we could not detect any CXCL13 at all in these areas, neither intracellularly nor extracellularly. CXCL13 accumulation therefore seems to be a scar-specific phenomenon. For that reason, the chemokine is indeed a possible candidate responsible for attracting B lymphocytes.

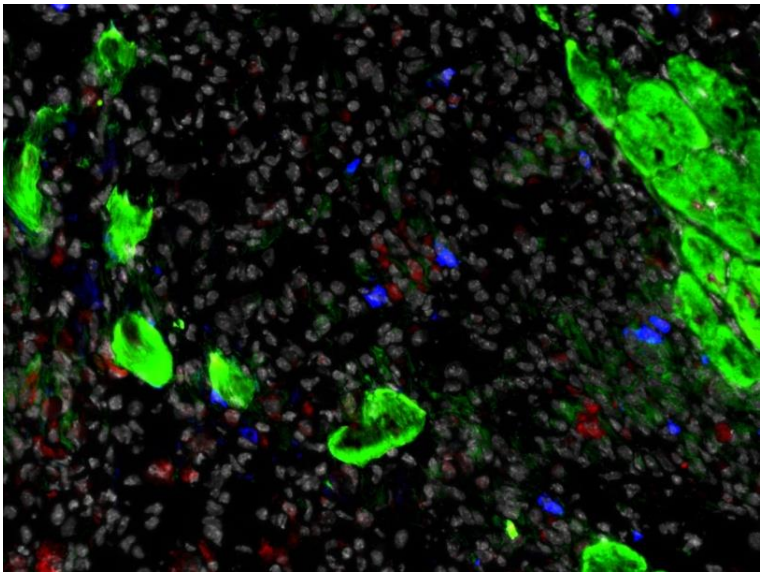

Figure 12: B cells ($B220^{+,}$ blue) and CXCL13 (red) in close localization (day 3 after MI) in border zone and scar. Cell nuclei are stained with DAPI (white) and colocalize with both B220 and CXCL13. Vital myocardium is phalloidin positive (green), while the scar is phalloidin negative (dark).

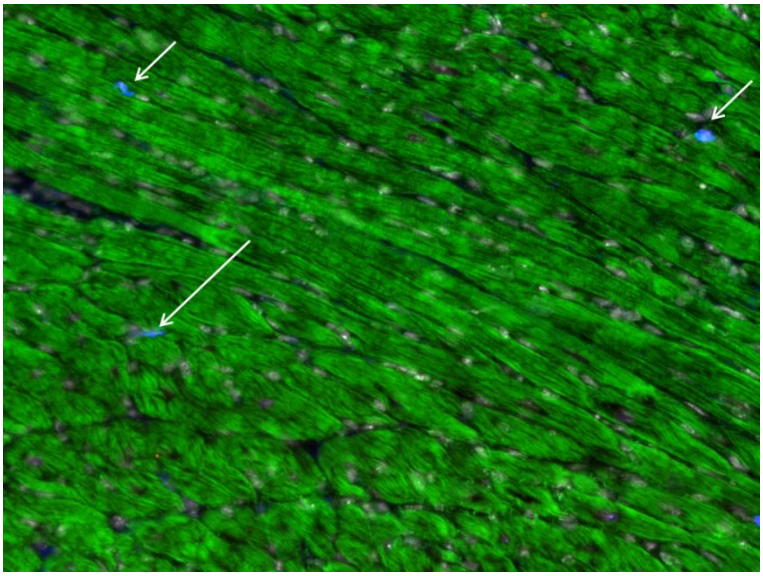

Figure 13: Only scarcely distributed $B220^{+}$ and $DAPI^{+}$ B cells (arrows) - and no detectable CXCL13 signal (red) - in the phalloidin-positive (green) septum (day 14 after MI).

3.3.2. Mechanism and kinetics of B-cell attraction through CXCL13

According to our findings in 3.1. Infiltration kinetics and localization of B cells after MI, B-cell infiltration of the scar reaches its peak around day seven. It is obvious that B cells immigrate into border zone and scar quite early after infarction. Therefore, we assume that CXCL13, if it was the key mediator for B-cell influx, must be evident in the respective zones even earlier than day five, maybe as early as day one or two after infarction.

We wanted to verify with a different method that CXCL13 is evident in the heart of post-MI mice. At first, we attempted to detect CXCL13 in a Western Blot. From the literature, it is known that the protein CXCL13 has a molecular weight of 11.927 kDA[89]. Using a prestained protein ladder (PageRuler™, Thermo Scientific, Waltham, USA), we could detect CXCL13 in heart protein extracts (2.2.2.6. Protein extraction). However, the primary and secondary antibody bound unspecifically in our experiments so that we found it difficult to exactly quantify CXCL13 contents in the different samples. Additionally, we observed a high variability of results in repeated experiment which revealed that findings were not in all cases reproducible due to methodical instabilities. We therefore regarded the method as inappropriate to compare different time points and were finally persuaded to abandon the method for further purposes.

To outline the kinetics of CXCL13 levels in the heart over time, we instead performed ELISA experiments as described in

2.2.2.9. ELISA. An ELISA is, compared to a Western Blot, also a much more sensitive technique. We had six mice undergoing an experimental myocardial infarction operation and six control mice that were sham-operated as described in

2.2.1.2. The mouse model of permanent myocardial infarction, each set for day one and day five. We checked not only scar and septum (MI mice) and compared them to sham

animals' hearts but also used the spleens of the sham animals as a positive control for CXCL13. In preliminary tests, we checked the efficiency and specificity of the commercial ELISA kit we used (Mouse CXCL13/BLC/BCA-1 Quantikine ELISA Kit, R&D Systems, Minneapolis, USA). As a negative control for CXCL13, we used and confirmed skeletal muscle. In all the thigh muscle samples which we produced, CXCL13 levels were not assessable (i.e. below detection level).

In our experiments, we could show that CXCL13 amounts increased in the scar tissue after myocardial infarction. On day one after infarction, there were significantly higher ($p < 0.01$) than in the sham-operated animals. The same applied to day five after myocardial infarction. If we compared day one to day five, we saw that CXCL13 amounts in the scar obviously decreased over time (Figure 14).

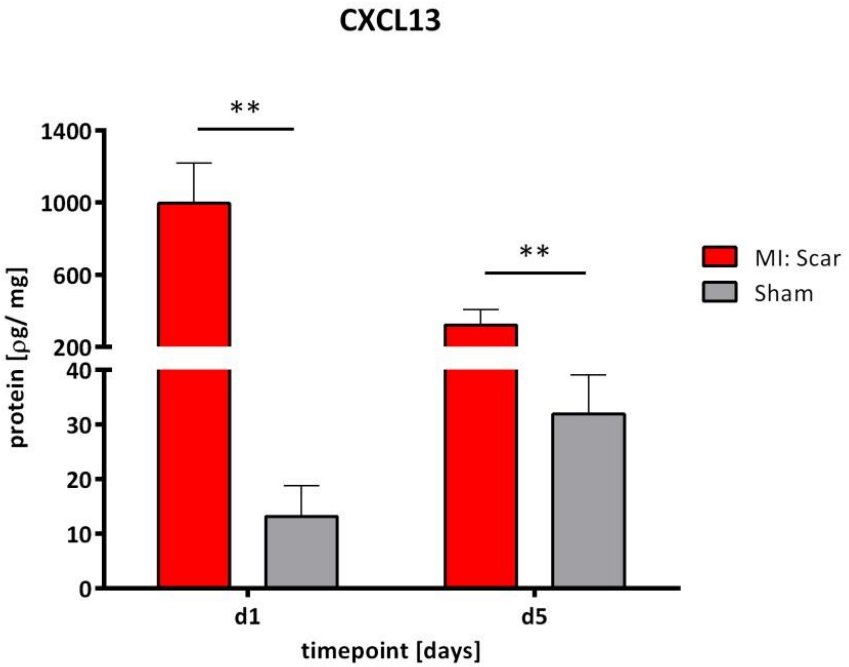

Figure 14: CXCL13 amounts in the scar tissue are significantly higher than in the hearts of sham-operated animals (d1), even five days after myocardial infarction (d5); p = 0.0013 (**) for d1, p = 0.0052 (**) for d5; n = 6/group.

Overall levels of CXCL13 (in ρg/mg protein) in the scar tissue were extremely high with approximately 1000 ρg/mg protein on day one after infarction and even significantly higher ($p < 0.01$) than in the respective septum (not infarcted myocardium) (Figure 15), indicating that there might have been a local concentration gradient between septum and scar, drawing B lymphocytes to the site of inflammation.

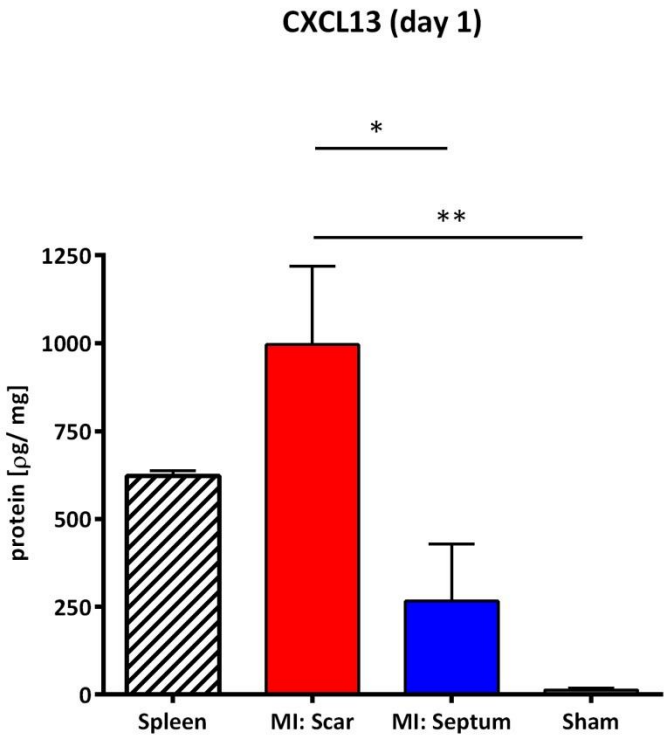

Figure 15: On day 1, CXCL13 is significantly higher in scar tissue than in the respective septum, p = 0.0248 (*), and sham animal, p = 0.0013 (**); n = 6/group.

On day five after infarction (Figure 16), CXCL13 levels in the scar of MI mice were still significantly higher than in the hearts of sham-operated mice ($p < 0.01$). Interestingly, chemokine levels, however, declined significantly below levels in the spleen ($p < 0.01$), which was not observed on day one (compare again Figure 15). CXCL13 levels in the spleen were relatively constant over time (600-650 ρg/mg) and therefore the spleen served as a normalizing control.

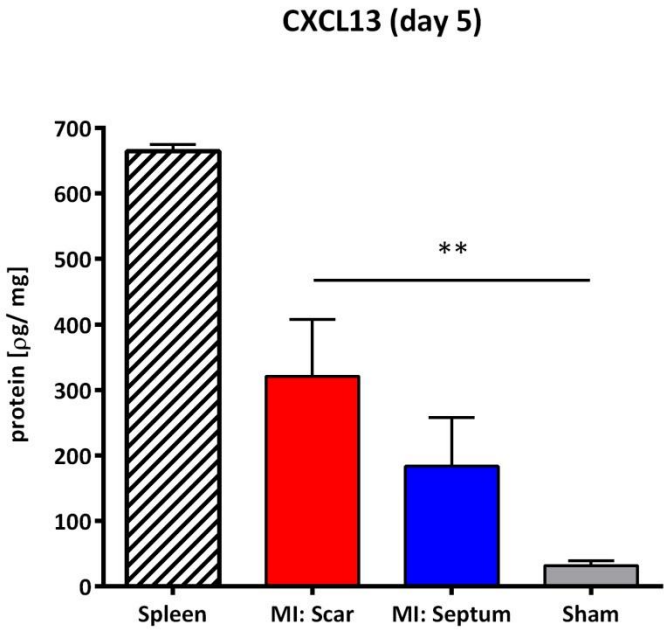

Figure 16: On day 5, CXCL13 amounts in scar tissue are significantly higher than in hearts of sham-operated animals, p = 0.0052 (**); the difference between scar and septum is, however, not significant anymore, p = 0.2639; n = 6/group.

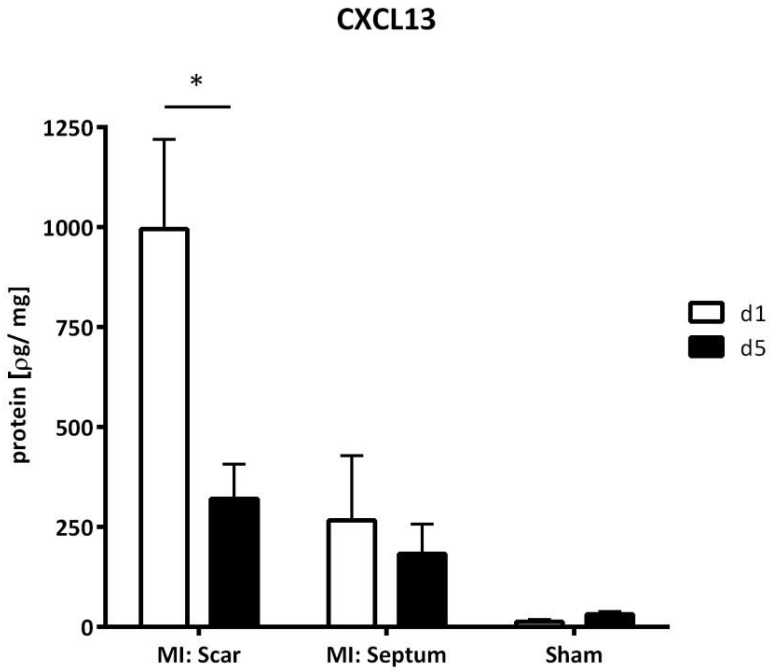

Figure 17: CXCL13 amounts in the scar tissue drop significantly between d1 and d5, indicating that most of the B-cell recruitment occurs early after infarction (and between d1 and d5), p = 0.0286 (*); n = 6/group.

As expected, CXCL13 levels in the scar dropped over time, i.e. in fact significantly by approximately 60 % between day one and day five (Figure 17). There were no relevant changes in the septum or in sham hearts.

Interestingly, CXCL13 expression seems to rise in the spleen at day five (compared to day one). This observation could be an indicator for systemic activation of the immune system in the context of myocardial infarction.

In conclusion, we observed a significant increase in the B-cell attracting chemokine CXCL13 in scar tissue after myocardial infarction compared to sham-operated animals, which was initially high (day one) and continually decreased over time (day five). As CXCL13 amounts were extremely low in animals without experimental myocardial infarction and at first even higher in the scar than in the spleen, upregulation of its

expression in response to an early hypoxic or inflammatory stimulus in the myocardial tissue is very likely.

3.3.2. Secretion of CXCL13 by monocytes and macrophages

From the literature it is already known that monocytes and macrophages invade the damaged myocardium after MI in great number and are an integral part of physiological healing[90].

To find out if monocytes or macrophages could also be the source of CXCL13 in our model of experimental myocardial infarction, we sorted monocytic cells ($CD45^+$, $CD11b^+$, $Ly6G^+$) from scar tissue on day five after MI. For RT-PCR, we extracted RNA from approximately 10.000 cells sorted from the scar (n = 1) on day five after myocardial infarction. Afterwards, we amplified the RNA in three rounds using the ExpressArt mRNA amplification Pico kit (AmpTec GmbH; Hamburg, Germany). In general, we compared gene expression on mRNA level in this sample with a control sample containing RNA of monocytic cells from the spleen. Gene expression was normalized on GAPDH and Actb. We had triplicates measured.

We found that monocytic cells from the scar highly expressed CXCL13 while in monocytes from naive spleen we could not detect any CXCL13 at all.

To confirm this finding, we stained cryosections of heart tissue (day three after MI) combining an anti-CD68 antibody with an anti-CXCL13 antibody. We found that both dyes indeed colocalized and there were cells positive for both markers (and $DAPI^+$) to be identified as CXCL13-containing monocytic cells. Indeed, we found several of those cells in the border zone and scar tissue of mice having undergone experimental myocardial infarction (Figure 18). In tissue segments spared from ischemia, we could however not detect those cells.

Putting our findings into context, it is most likely that CXCL13-secreting monocytic cells are proinflammatory, as they could be detected early after MI (at the latest on day three), and contribute to tissue invasion e.g. by attracting B lymphocytes via their CXC receptor 5 (CXCR5).

Of course, a second approach would be necessary to confirm that it is, indeed, monocytic cells that are the source of CXCL13.

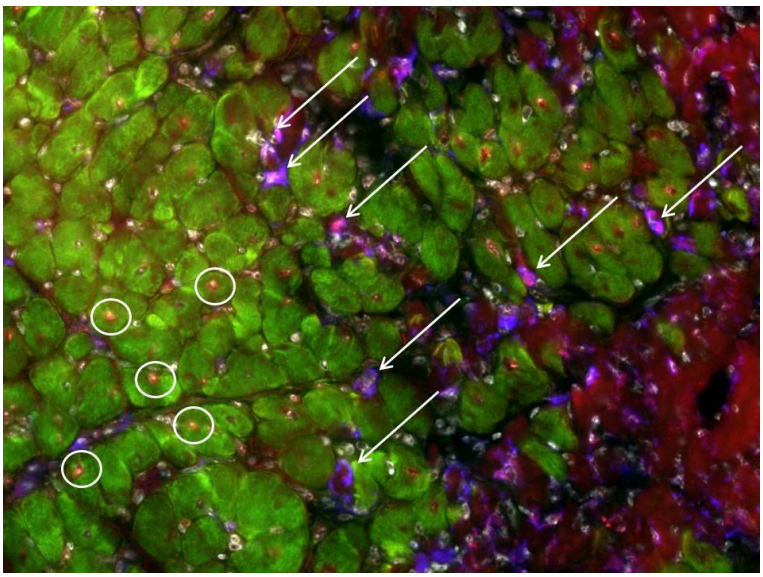

Figure 18: CD68 (blue) and CXCL13 (red) colocalize in the border zone between scar and phalloidin-positive (green) vital myocardium (arrows). There are also some $CXCL13^{+}$ cells that are $CD68^{-}$ (circles).

We could not find any evidence for elevated levels of CCL19 or CXCL12 in the scar in RT-PCR experiments.

3.4. Therapeutic approaches

3.4.1. CXCL13 neutralization

Consequently, and to verify our earlier findings, we attempted to prevent B cells from infiltrating the myocardium by administering an anti-CXCL13 antibody to neutralize CXCL13. In the literature, a CXCL13 antibody is described (mouse CXCL13 MAb, cl1 143614; R&D Systems, Minneapolis, USA), neutralizing CXCL13 within 24 hours of administration and thereby causing a disruption of tissue architecture in the spleen. The effect is dose-dependent and includes a loss of primary follicles, secondary follicles and GCs as well as a ring-building of B cells and deprivation of FDC. Sustained disruption was observed up to 20 days after application[91].

In our experiment, we compared mice undergoing a treatment prior to MI induction with the above described antibody (200 µg i.p.) with a control group (n = 6) receiving a placebo antibody instead. Three hours after antibody administration, myocardial infarction was induced by ligature of the LAD.

Three days after treatment and MI induction, the mice were euthanized and their body as well as heart and spleen weights were measured.

Afterwards, frozen sections were produced from harvested hearts (concentric ring of the right and left ventricle containing scar and septum) and spleens and stained with phalloidin as well as B220 (compare

2.2.2.1. Histology and immunofluorescence microscopy and 3.1. Infiltration kinetics and localization of B cells after MI) to tag B cells. Our assumption was that a neutralization of CXCL13 would lead to a reduced influx of B cells into the heart and therefore also to fewer total B cell numbers in the infarct area. We therefore counted B cells in a fluorescence microscopy evaluation and referenced their numbers to either the

phalloidin-positive tissue area (septum: intact myocardium) or the phalloidin-negative scar tissue area.

We found that in mice treated with the anti-CXCL13 antibody (verum) there were indeed significantly fewer B cells in phalloidin negative areas than in mice treated with the placebo antibody (Figure 19). Additionally, there is a significant difference in the B-cell number between phalloidin negative and positive area in the placebo group, while this disparity is resolved upon CXCL13 neutralization in the verum group demonstrating that the treatment is effective.

Interestingly, B-cell numbers in the phalloidin positive tissue are comparably low in animals receiving verum and animals receiving the placebo antibody. This supports the idea that mostly the non-resident B cells immigrating from the bloodstream into the scar tissue are affected by the therapy, whereas frequencies of tissue-resident B cells appear to remain stable over time and are unaffected by antibody treatment.

For statistical analysis, we used – in each case – an unpaired t test to compare verum with placebo because histological evaluations for each group were independent experiments. And even within the group, phalloidin negative and positive areas are not comparable and therefore do not require a paired t test.

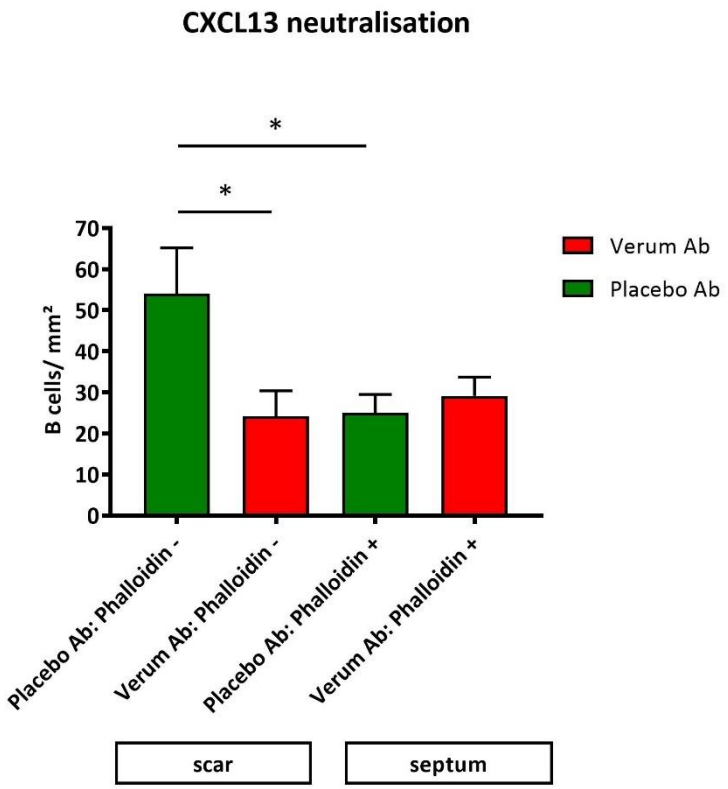

Figure 19: Treatment with a CXCL13-neutralizing antibody reduces B-cell numbers in the scar tissue significantly, p = 0.0466 (*). The CXCL13 gradient between phalloidin negative and positive tissue in the placebo group (green bars), p = 0.0415 (*), is eliminated by the treatment with the CXCL13-neutralizing antibody (red bars); n = 5.

Next, we wanted to find out if the treatment of mice with a CXCL13-neutralizing antibody also minimizes the infarct area. Our assumption was that a reduced B-cell influx after myocardial infarction might thereby improve cardiac function and finally be beneficial for the overall outcome.

Therefore, we examined 48 wild-type mice (in a double-blind setup). On day seven and 28, echocardiography was performed to assess functional parameters of the heart. On day 28, all animals were euthanized and the hearts harvested (primary endpoint).

30 animals survived the procedure of experimental infarction until the primary endpoint and could be included in the final evaluation. Out of those, 17 had received treatment with the anti-CXCL13 treatment and 13 control animals had been treated with an isotype

control instead. In the verum group, four animals had died because of left-ventricular rupture because of a very large infarct. In the placebo group, eight animals had died for the same reason, particularly in the first days after experimental infarction, between days three and six (Figure 20).

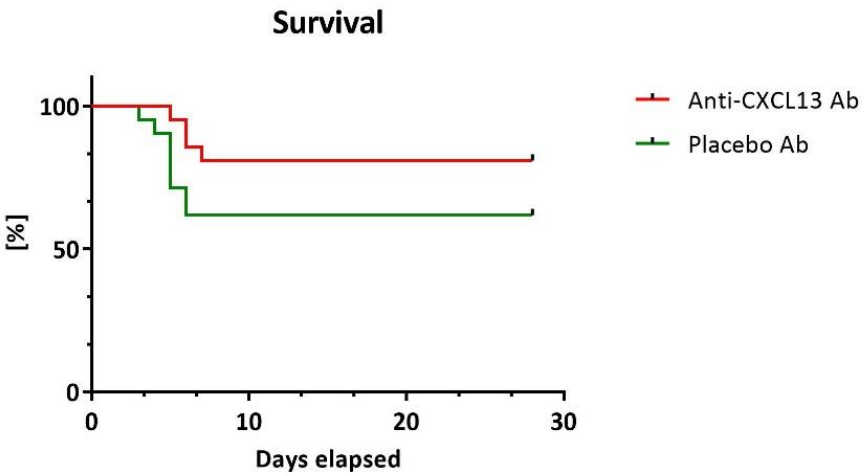

Figure 20: The survival of mice treated with the anti-CXCL13 antibody is by trend better than that of control mice treated with placebo antibody, the difference is, however, not statistically significant; long-rank (Mantel-Cox) test: p = 0.1315.

Concerning left-ventricular weight in relation to body weight as an indicator for hypertrophy, a common long-term consequence of myocardial infarction[49], we could not find a difference between the groups (Figure 21).

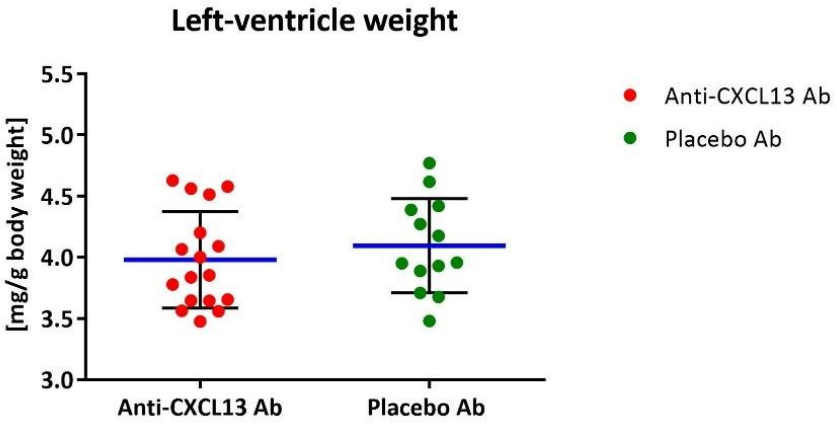

Figure 21: Animals treated with the anti-CXCL13 antibody do not have a reduced left-ventricular weight compared to animals treated with the placebo antibody.

Next, we evaluated the infarct size of animals in both treatment groups based on histologic sections stained with PSR (see also 2.2.2.2. Conventional histology). Unfortunately, we could only include five animals in the anti-CXCL13 group because of several reasons. Three animals had to be excluded because of post-operative granulomatous inflammation of the thoracic surgical scar. Nine animals showed none or only a diminutive infarct area. In some other cases, sections were disrupted due to technical problems and could therefore not be analyzed.

In the control group, we could determine the infarct size of nine animals. Here again, four animals had no infarction histologically.

We must furthermore note that infarct sizes were in general very heterogeneous (see Figure 22). Usually, only infarct sizes > 30% are convincing and will be included in further analyses. In our case, however, only two animals in the anti-CXCL13 group and five animals in the placebo group reached this objective. This might have been due to operational circumstances and inequalities, but we can only speculate here. Altogether, for the reasons named above, 12 animals in the verum group and four animals in the placebo group could not be considered.

In conclusion, also allowing infarct sizes < 30 %, we saw no difference between verum and placebo group (Figure 22).

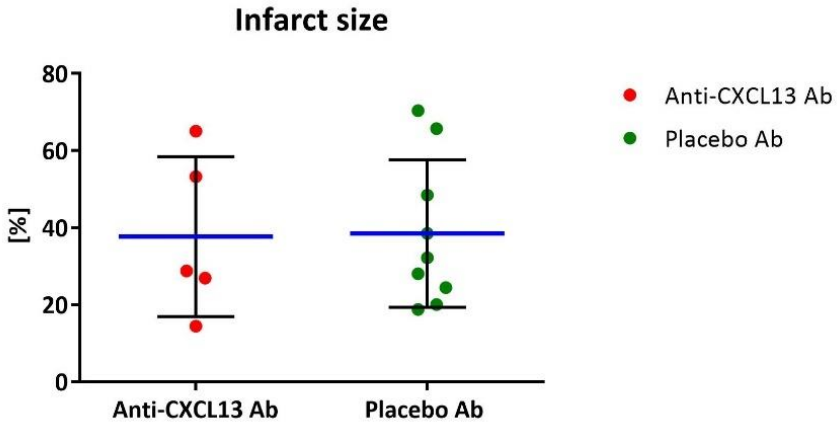

Figure 22: Infarct sizes in both groups differ enormously, a difference in between both groups cannot be described.

As described above, all animals were evaluated echocardiographically on day seven and day 28 after myocardial infarction. There were no statistically significant differences between the groups concerning the gathered parameters.

One noteworthy result might be the tendency to smaller infarct sizes in the group treated with the CXCL13-neutralizing antibody (eight animals) as compared to the placebo group (one animal) on day 28 after infarction. In that latter group, most animals had medium-sized infarcts (seven animals).

Exemplarily and because of their clinical relevance, we wanted to have a closer look at the parameters AP EDA, anterior-posterior end-diastolic area, and AP FS 2D, anterior-posterior fractional shortening in 2D mode. The measurements for both parameters are mostly comparable in the groups and there are no statistically significant differences.

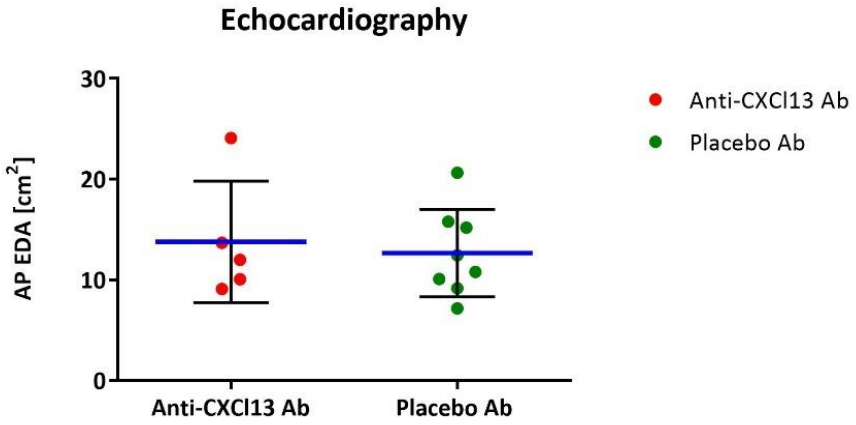

Figure 23: Anterior-posterior end-diastolic areas [cm^2] of both groups showing no significant differences.

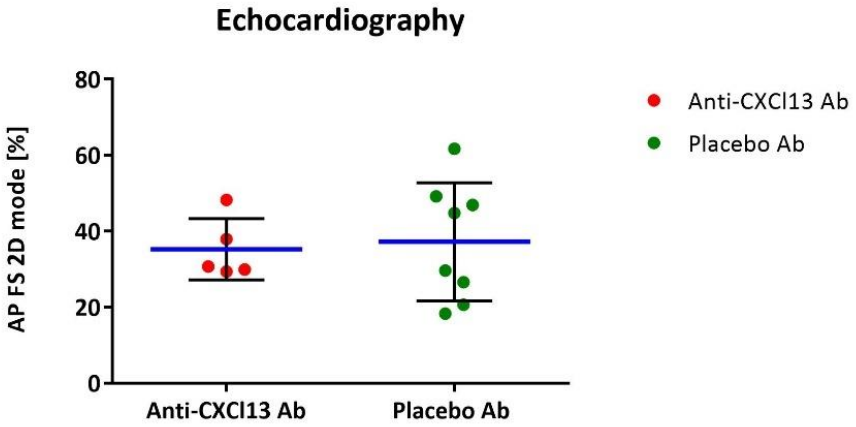

Figure 24: Anterior-posterior fractional shortening [%] with comparable results in both groups.

In conclusion, echocardiography parameters of treated animals do not seem to show an improved heart function compared to the placebo group, neither do measured data for left-ventricular hypertrophy or infarct size. Concerning the survival of animals, subjects treated with the anti-CXCL13 antibody might show a tendency towards improved survival.

4. Discussion

This study addressed the role of B lymphocytes in a mouse model of myocardial infarction.

The collected data show that B cells accumulate in the ischemic areas early after myocardial infarction and peak on day seven. Our findings indicate that B-cell trafficking into the heart is mediated by the chemokine CXCL13 which can be detected in the scar already at day one after infarction. As a potential source of CXCL13 we consider monocytic cells. CXCL13 neutralization prevented infiltration of B cells into the heart which led by tendency to improved survival of these animals compared to control-treated mice.

4.1. B lymphocytes in the heart after myocardial infarction: Possible functions and interactions

The involvement of the immune system in cardiovascular diseases has been known for a long time. Hypoxia is one stimulus of immune activation resulting in molecular alterations known as sterile inflammation. While the role of the innate immune system has already been understood quite comprehensively, fewer details are known about the adaptive immune system and especially its cellular components.

At the very beginning of our work, we observed that B lymphocytes accumulated in the myocardium after experimental myocardial infarction, in the area of myocardial necrosis as well as in the so-called border zone between healthy and damaged areas. Analyzing B-cell counts over time, we found that they peaked at day seven.

Although we found it difficult to fully characterize those B cells concerning all their subsets, we saw that most of them were in fact mature B cells. Plasma cells, putatively

secreting specific antibodies against cardiac antigens, could only scarcely be encountered.

Meanwhile, there is experimental evidence from a recent study indicating that B-cells might modulate the response of the innate immune system to myocardial injury[56]. Zouggari et al. describe an increased tissue damage as well as an impaired post-infarction cardiac function due to B cells infiltrating the myocardium which peaked, in their results, at day five after infarction. The authors also found that these cells were mostly mature B cells and initiated the mobilization of pro-inflammatory Ly6C^{high} monocytes into the heart by production of the cytokine CCL7. CCL7 is responsible for monocyte attraction and the regulation of macrophage function likewise[92]. Prolonged or increased attraction of Ly6C^{high} monocytes has been made accountable for an impeded healing process[93].

In fact, there are two phases of monocyte differentiation after myocardial infarction. The first period after MI is dominated by pro-inflammatory monocyte-derived macrophages, while in the second phase anti-inflammatory macrophages prevail.

Ly6C^{high} monocytes dominate the inflammatory phase early after myocardial infarction (days one to four) and can develop into M1-like polarized tissue macrophages which can lead to deteriorated wound healing[21]. Anti-inflammatory macrophages (among others derived from Ly6C^{low} monocytes), however, prevail in the second phase after myocardial infarction (days five to 16) where repair processes are ascendant. Putting their findings into context, the authors claim that B lymphocytes, indeed, negatively contribute to post-infarction healing by regulating monocyte attraction and differentiation within the myocardium.

The group showed that Ccl7-deficient mice (*Ccl7*$^{-/-}$) had an improved cardiac function after myocardial infarction – compared to wild-type mice. Cardiac function was assessed by echocardiography measuring fractional shortening (FS) which was increased in the Ccl7-deficient mice compared to wild-type mice 14 days after myocardial infarction.

Besides, complete B-cell depletion reduced infarct sizes as well as collagen content in

the investigated animals, an effect that could be mitigated by transfer of wild-type but not Ccl7-deficient B lymphocytes. It is, however, unlikely that all post-infarction B-cell effects on the myocardium are mediated by Ccl7.

To conclude, fewer B cells in the scar tissue could improve cardiac outcome after myocardial infarction by reducing the influx of Ly6C^{high} monocytes and thus limiting pro-inflammatory macrophage accumulation which is associated with a negative prognosis.

As a consequence and to control B-cell mediated effects of monocytic cells, Zouggari et al. suggest a depletion of B cells through either a CD20-specific antibody, rituximab, or a Baff-specific antibody, now commercially available as belimumab[94]. Baff, the B-cell activating factor of the TNF family, is an important survival and developmental factor of B cells, usually secreted by neutrophils, monocytes and macrophages. Patients with elevated blood levels of either Ccl7 or Baff are believed to have a higher risk of sudden cardiac death or reoccurrence of MI.

As total B-cell depletion is associated with long-term B-cell aplasia and, thus, immunodeficiency[95], we pursued a different strategy: The neutralization of the B-cell attracting chemokine CXCL13 (see also 3.3. The chemokine CXCL13 and its role in myocardial infarction and 4.2. CXCL13 and its role in attracting B cells into the infarct area: therapeutic implications). We also believed that this treatment is more tolerable in terms of side and adverse effects.

Apart from the fact that we found B cells in the infarcted heart, the precise functions of them remain elusive and would need further investigation. They could interact with T cells. Besides, B cells can also act as either antigen-presenting cells or co-stimulatory factors. It would also be interesting to identify cardiac antigens presented after myocardial infarction. It is likely that antigen presentation takes place not only in the heart-draining lymph nodes but also directly at the site of infarction. Although we did not yet investigate these interactions, it would be interesting to co-stain T and B cells in the myocardium, for example. Additionally, it would be necessary to also check the B cells' activation status as there are T-cell dependent and independent ways of B-cell activation[96].

As we could only detect a very small number of antibody-secreting B cells (plasma cells) in our heart samples, it is more likely that the specific immune response is a systemic matter in myocardial infarction. Further investigations concerning systemic immune activation after myocardial infarction are also pending.

4.2. CXCL13 and its role in attracting B cells into the infarct area: therapeutic implications

While Zouggari et al. did not focus on the mechanism of B-cell attraction into the damaged myocardium, this question was central to our work. We therefore investigated several molecular pathways including chemokines known for B-cell trafficking: CXCL13, CXCL12 and CCL19.

The chemokine CXCL13 was soon in the focus of our attention as a promising candidate responsible for the recruitment of B cells into the injured myocardium. CXCL13 is a well-known homeostatic chemokine active in the spleen, where it coordinates – through its receptor CXCR5 – the movement of B cells.

CXCL13 can function as a mediator preventing apoptosis as well as inflammation which has been shown e.g. in atherosclerosis by Smedbakken et al. in 2012[82]. In humans, monocytes and macrophages were found to secrete CXCL13 with beneficial local as well as systemic effects, among them plaque stabilization. The mechanisms could however not be clarified comprehensively. Recently, the same group published a paper claiming similar ramifications also in myocardial infarction[97].

In our experiments, we could prove that CXCL13 expression increased in the heart early after myocardial damage. We made similar observations in splenic tissue. In this case, however, expression increased only at day five, i.e. with latency. This indicates that there is first local and consecutively systemic immune activation after myocardial infarction.

Physiologically, CXCL13 is active in secondary lymphatic organs just like the Peyer's patches in the small intestine or lymphatic tissue in tonsils or the skin. At these sites, foreign or auto-antigens are presented to naive lymphocytes, activate them and thereby induce an adaptive immune response, specific against a certain antigen. Lymphocytes that have been primed like this are then able to patrol blood and other compartments and organs to encounter and eliminate dangerous antigens or, in rare cases, self-antigens.

CXCL13 is responsible for the movement (or trafficking) of B cells in the germinal centers (GC) of lymph follicles. It specifically interacts with the receptor CXCR5 expressed by centrocytes in the light zone of the GC[98].

Centrocytes are mature B cells that have, in contrast to centroblasts, already undergone somatic hypermutation (SHM) which takes place in the outer, dark zone of the GC. SHM describes the modification of the IgV region of the rearranged antigen receptor at the B-cell surface during an immune response. CXCL13 in secondary lymphoid organs is secreted mainly by FDCs[99]. Upon FDC ablation in the GC, GC lose their homogeneity and eventually disappear, supposedly because of missing CXCL13.

CXCL13 is not only responsible for recruitment and homing of B cells to lymphoid tissue, but is also essential during embryogenesis for the development of most lymph nodes and the Peyer's patches. Mice deficient in CXCL13 lack all lymph nodes except for the mesenteric lymph nodes[91]. CXCR5-deficient mice show a severely disrupted splenic architecture and CXCR5-deficient B cells are unable to migrate towards a CXCL13 gradient[100]. Various studies indicate that CXCL13 overexpression, however, leads to lymphoid neogenesis and B cells can also be attracted towards ectopic CXCL13 expression. As lymphoid neogenesis also plays a role in inflammatory and autoimmune diseases such as rheumatoid arthritis, we assumed a potential role of CXCL13 also in our model of myocardial infarction (see also 4.1. B lymphocytes in the heart after myocardial infarction: Possible functions and interactions). Accordingly, we found mostly mature B cells in the border zone and scar after myocardial infarction. All mature murine B cells express

the receptor for CXCL13, CXCR5, and can therefore move towards a CXCL13 gradient, just like centrocytes in the spleen[101].

More generally speaking, distinct B cell precursors or subsets express specific chemokine receptors according to their function. For example, immature B cells migrate from the bone marrow into the spleen because they carry a receptor called CXCR4 responsive for the chemokine CXCL12 which is highly expressed in the red pulp[102]. As described before, $CXCR5^+$ naive B cells are attracted by CXCL13 secreted in the white pulp. Memory B cells are attracted by $CCL20^+$ epithelial cells through their receptor CCR6[108]. Likewise, B cells with the appropriate receptor can home specifically to various tissues. Additionally, the expression of these chemokine receptors can be influenced post-transcriptionally by either TLR stimulation or the activation of BCRs or CD40[103].

We could show not only that CXCL13 levels increased in the murine heart after myocardial infarction but also that its expression was especially higher in the scar tissue, already at day one after myocardial infarction. In our histological studies, we found that the B cells in the scar tissue were found next to CXCL13. This suggests, once again, an interaction.

To confirm our findings that CXCL13 indeed played a role in attracting B cells to the site of myocardial infarction, our idea was to prevent the influx of B lymphocytes into the infarct area by therapeutic neutralization of CXCL13.

Although the neutralization was successful, we did not see any significant beneficial effects concerning infarct size, heart function or survival. We would on the one hand need higher numbers of animals and maybe also an extended period of observation to capture also the long-term results (e.g. remodeling, development of heart failure). On the other hand, the fact that there are no differences between the groups could also be because we investigated only animals surviving until the end of the study. For sure, only the fittest animals – with maybe comparable infarct sizes and similar cardiac function – reached that endpoint. If this is true, the intriguing result is, in fact, the improved survival rates in the group treated with the anti-CXCL13 antibody.

Besides local effects, one must also consider the systemic effects of immune activation and rising cell counts. We could, for example, also detect rising numbers of B cells in the spleen. From other publications, it is known that also in the heart-draining lymph nodes different immune cells accumulate and possibly interact after myocardial infarction[66]. It would be interesting to examine these interdependencies more closely. The replenishment of cells is possible because the bone marrow is activated after myocardial infarction – another field of research still only partly understood[93].

In our opinion, a treatment of myocardial infarction in mice or humans with a highly specific therapy (e.g. with an anti-CXCL13 antibody) is, however, much more favorable than a general immunomodulation. Because an antibody therapy specifically targets one antigen, it is accompanied by fewer side effects.

This is, because CXCL13 does not completely inhibit all types of B cells but only those equipped with CXCR5. Mice genetically lacking either one of these factors show abnormal embryonic development of lymph nodes and antibody-secreting B cells, for example. If CXCL13 is however blocked postnatally, i.e. in a fully developed immune system, systemic effects cannot be observed to that extent. In fact, inhibition or neutralization of CXCL13 in adult mice leads to a structural alteration of lymphoid follicles within the first day of administration. Primary follicles dissolve, B cells build rings around T-cell rich zones in the spleen and follicular dendritic cells are even depleted. Meanwhile, there are fewer changes to be observed in the marginal zone[91]. Consequently, splenic secondary follicles, networks of FDC and GC are lost.

Special T cells are also known to be $CXCR5^+$ and are therefore affected by CXCL13 neutralization: T follicular helper (Tfh) cells, a subset of regulatory T cells (T_{reg} cells). They are known for providing necessary costimulatory signals to B cells[104] and are important for germinal center formation, B-cell maturation as well as the production of antibodies and memory B cells[105]. In autoimmune diseases such as Sjogren's syndrome[106], dermatomyositis[107] and systemic lupus erythematosus[108] in humans and mice, elevated frequencies of Tfh cells have been reported and are associated with higher antibody

levels. Notably, Tfh cells also produce IL-21, a cytokine responsible for proliferation and differentiation of B cells, among other things[109].

Taking these facts into account, a neutralization of CXCL13 could land a double hit, inhibiting detrimental B- and T-cell effects after myocardial infarction.

Interestingly, the humoral immune response is not restricted upon administration of anti-CXCL13 antibodies[91]. Instead, anti-CXCL13 treatment impedes the activation of NF-κB2 and IκBα, factors known for their pro-inflammatory impact on gene regulation. Apart from that, this treatment has many other inflammation-resolution effects[101]. By contrast, treating humans with an anti-CD20 antibody might still affect many aspects of immune defense as it targets pre-B cells, immature B cells, naive B cells, and memory B cells at the same time. Systemic side effects of the therapy might include mild and transient phenomena such as fever, headache and nausea as well as more severe symptoms like acute respiratory distress syndrome (ARDS), congestive heart failure, myocardial infarction itself and sepsis as well as the reactivation of latent infections, among them hepatitis, CMV and EBV infections[110].

For our work, besides from T and B cells, monocytic cells were of special importance. After thorough literature research, we had identified monocytic cells as a potential source of CXCL13 underlining again the necessity of restricting the B-cell invasion into damaged tissue. Because, if monocytes indeed produced CXCL13 and attracted B cells which, in turn, were responsible for the attraction of monocytes, this is a vicious circle to be disrupted to improve healing after myocardial infarction.

Under steady-state conditions, follicular dendritic cells are the major source of CXCL13 in lymphatic organs and at deviant sites of lymphoid tissue development[111, 112] while monocytic cells in blood and spleen do not produce or secrete CXCL13. In inflammatory lesions, however, this is possible[113]. At least in human rheumatoid arthritis and ulcerative colitis, where lymphoid neogenesis has been generally reported[78], most CXCL13-positive cells are of monocytic origin and are not embedded in a germinal center-like structure but rather grouped closed to small aggregations of B cells where no FDCs are encountered[113]. As an additional finding, $CD4^+$ T cells also produce CXCL13

in human rheumatoid synovitis[114]. Their role is potentially not only in ectopic lymphoid neogenesis but also in attraction of B cells and circulating T follicular helper cells.

Another possible side effect of the neutralization of CXCL13 could be the off-site and systemic effects on the murine immune system. As mentioned earlier, the treatment of adult mice with an anti-CXCL13 antibody led to the disruption of splenic structures such as loss of primary and secondary follicles, FDC as well as GC, a condition that remained until 20 days after initial treatment. The marginal zone was, interestingly, not affected[91].

We believe, however, that in our case drug doses were far too low to provoke such effects. In histologic studies, we could not detect any morphological alterations in spleens of mice having experienced a CXCL13 neutralization. The applied doses were sufficient though to induce the desired therapeutic effect, i.e. prevent the immigration of B lymphocytes into the damaged myocardium.

The chemokines CXCL12 and CCL19 were finally left out of consideration because in RT-PCR experiments we could not detect elevated levels of these two cytokines in the heart tissue. Nevertheless, we cannot rule out that there might also be other chemokines recruiting B cells – maybe more specific and even not yet described B-cell subsets.

In conclusion, our findings suggest that the neutralization of CXCL13 could be a method to modulate immune responses after MI in a favorable way without compromising humoral immune responses in general. However, further research is necessary to characterize processes after myocardial infarction in the heart – and in secondary lymphatic organs as well as the bone marrow.

4.3. B cells after myocardial infarction in a clinical context

In their paper from 2013, Zouggari et al. claim that B cells worsen the clinical outcome after myocardial infarction in the mouse. The depletion of B cells with an anti-CD20

monoclonal antibody would consequently lead to reduced inflammation, hence smaller infarct sizes and an overall improved heart function[56].

To be precise, we cannot directly compare a B-cell depletion regime with a CXCL13 neutralization.

In our studies, mice treated with an anti-CXCL13 antibody showed improved survival rates. However, when comparing the survivor animals, there were no significant differences between the groups when we assessed heart function echocardiographically.

Consequently, it would be necessary to perform systematic studies also in humans, especially with non-invasive methods that can be used in living individuals to detect and count e.g. B lymphocytes in the heart after myocardial infarction. Imaging methods such as leucocyte or B-cell PET scans are – in principle – also available in humans. In the future, they might be useful for risk stratification or to define different therapy groups after myocardial infarction.

A therapy with a CXCL13-neutralizing antibody seems on the one hand practical and on the other hand relatively precise and effective if initiated preferably early after the incident.

A problem worthy to discuss might however be the unspecific inactivation of B cells, presumably including also regulatory B cells (B_{reg}). This B-cell subtype is beneficial in mouse models of inflammation, transplantation, cancer and in sterile inflammation, e.g. in autoimmune diseases, as it negatively regulates the immune response. B_{reg} cells produce regulatory cytokines, among them IL-10 and directly interact with pathogenic T cells[116]. One can imagine positive effects of B_{reg} cells also in myocardial infarction. To prevent a complete loss of regulatory B cells, it would probably be advisable to perform an immunomodulation in the sense of a B-cell depletion or a CXCL13 neutralization only in the first, inflammatory phase after myocardial infarction and to spare the second, anti-inflammatory phase, where regulatory B cells are supposedly of more importance.

When translating our findings into the clinic, we must finally also consider different preconditions in the patient population. What if a patient had an autoimmune disease and myocardial infarction simultaneously? What if he suffered from an acute active or chronic infection? What about immunosenescence?

Immunosenescence describes the fact that with aging, the immune system changes. Among other modifications, the bone marrow might become partly insufficient in delivering extra immune cells in case of inflammation. Besides, lymphocytes could be negatively affected in their development, maturation, function and migration[117]. This implies also an altered reaction to both myocardial infarction and the potential therapy.

In a recent publication, Ramos et al. found out that myocardial aging is aggravated by T cells. According to their findings, $CD4^+$ T cells decisively contribute to myocardial inflammation and consecutive functional impairment in aging mice[118]. The authors could also verify that even in the healthy heart, B and T lymphocytes can genuinely be found. Apparently, cardiotropic T cells are constitutively expressed in old mice. It remains to be figured out if the same could be true for B cells. After all, alterations in the immune system due to aging would also have to be considered in cardioimmunologic research – not least because in humans, heart attacks rather occur in senior individuals.

5. Abstract

Myocardial B-cell infiltration after LAD occlusion in mice is driven by CXCL13

After myocardial infarction, the immune system is activated and regulates wound healing and remodeling processes in the heart.

While the role of T cells has been elucidated already[66], the function of B cells in myocardial infarction remained relatively unclear until now. It is, however, already known that B cells are of importance in healing processes in other tissues, for example in the skin[67] .

Our studies therefore addressed the role and function of B cells in healing and early remodeling processes in the myocardium after infarction.

Under physiological conditions, only few B cells can be found in the heart. After myocardial infarction, however, which we modelled with a permanent ligation of the left anterior descending artery (LAD) in C57BL/6J mice, we could demonstrate that B lymphocytes accumulate in the early phase after tissue injury (days one to seven) in the myocardium.

To detect B cells, we performed immunofluorescence stainings on cryosections of infarcted hearts using an anti-B220 antibody. Quantitative analysis of tissue infiltration revealed that B cells peaked at day seven. In flow cytometry, we further characterized the B cells infiltrating infarcted tissue. We found that most of them were mature B cells (IgM^+, IgD^+).

Next, we wanted to outline a potential mechanism responsible for B-cell infiltration to the site of tissue injury. We therefore performed ELISA experiments revealing that CXCL13 was upregulated in scar tissue.

Antibody-mediated neutralization of CXCL13 verifiably attenuated B-cell infiltration. Treated mice also showed – in the tendency – smaller infarct sizes and an improved survival.

In conclusion, we could show that B lymphocytes infiltrate the myocardium after MI in mice following a local CXCL13 gradient and that it is, most likely, beneficial to inhibit this process.

Die Infiltration des Myokards durch B-Lymphozyten nach Ligatur der linken Koronararterie im Mausmodell wird durch CXCL13 verursacht

Nach einem Herzinfarkt wird das Immunsystem aktiviert und bestimmt die Wundheilung sowie das *Remodeling* im Herzen.

Während die Rolle von T-Zellen [dabei] bereits relativ gut untersucht ist[66], war die Funktion von B-Zellen beim Myokardinfarkt bis heute relativ unklar. Man weiß bisher allerdings, dass B-Zellen eine wichtige Rolle in Heilungsprozessen in anderen Geweben spielen, z.B. in der Haut[67].

Unsere Untersuchungen beschäftigten sich daher mit der Rolle und Funktion von B-Zellen nach experimentellem Herzinfarkt im Mausmodell.

Unter physiologischen Bedingungen finden sich nur wenige B-Zellen im Herzen. Nach Herzinfarkt, den wir mithilfe einer permanenten Ligatur der linken Herzkranzarterie in C57BL/6J-Mäusen induzierten, konnten wir jedoch zeigen, dass B-Zellen in der frühen Phase nach Gewebeschädigung (Tag eins bis sieben) im Myokard akkumulieren.

Um B-Zellen zu detektieren, führten wir Immunfluoreszenz-Färbungen mit einem monoklonalen Anti-B220-Antikörper auf Gefrierschnitten des Herzens durch. Eine quantitative Auswertung der Gewebeinfiltration ergab, dass die Anzahl der B-Zellen an Tag sieben ihren Höhepunkt erreicht. In durchflusszytometrischen Untersuchungen charakterisierten wir [anschließend] die das infarzierte Gewebe infiltrierenden B-Zellen (weiter). Wir stellten dabei fest, dass es sich bei den meisten dieser Zellen um reife B-Zellen (IgM^+, IgD^+) handelte.

Als nächsten Schritt wollten wir einen möglichen Mechanismus, der die B-Zell-Infiltration am Ort der Gewebeschädigung erklärt, umreißen. Wir führten daher ELISA-Messungen durch, die ergaben, dass CXCL13 im Narbengewebe hochreguliert war.

Eine Antikörper-vermittelte Neutralisation von CXCL13 konnte nachweisbar die B-Zell-Infiltration hemmen. So behandelte Mäuse zeigten – in der Tendenz – kleinere Infarktgrößen und ein verbessertes Überleben.

Zusammenfassend konnten wir somit zeigen, dass B-Lymphozyten nach Myokardinfarkt in der Maus das Myokard aufgrund eines lokalen CXCL13-Gradienten infiltrieren und dass es höchstwahrscheinlich vorteilhaft ist, diesen Prozess zu unterbinden.

6. Acknowledgements/Danksagung

An dieser Stelle möchte ich mich bei allen Personen bedanken, die mich während der Anfertigung meiner Doktorarbeit begleitet und unterstützt haben.

In allererster Linie gilt mein Dank meinem Doktorvater Herrn Prof. Dr. med. Stefan Frantz für die Ermutigung zu dieser Arbeit, für die gute Betreuung und den stetig vermittelten Ansporn, sich wissenschaftlich zu betätigen und weiterzuentwickeln. Für sein Vertrauen in mich und auch für seine persönliche Förderung bin ich sehr dankbar.

Herrn PD Dr. med. Ulrich Hofmann danke ich herzlich für die hervorragende fachliche Betreuung, vor allem gegen Ende der experimentellen Arbeit, sowie beim Verschriftlichen dieser Arbeit.

Meinem initialen Betreuer Georg Wedekind danke ich vor allem für seine gute Lehre sowie für seine kritische und ständig hinterfragende Herangehensweise an wissenschaftliche Fragestellungen, die er mir vermittelt hat. Ich konnte außerdem sehr eigenständig arbeiten, eigene Ideen entwickeln und auch umsetzen. Das wäre natürlich auch ohne die finanzielle Unterstützung des Else-Kröner-Forschungskollegs Würzburg nicht möglich gewesen. Vielen Dank auch dafür.

Herrn Prof. Dr. rer. nat. Albrecht Müller danke ich für die konstruktiven Anmerkungen zu meiner Arbeit.

Herrn PD Dr. med. Niklas Beyersdorf herzlichen Dank für die kurzfristige Übernahme der Zweitbetreuung meiner Arbeit und für die hilfreichen und stringenten Abschlusskorrekturen.

Der Medizinischen Fakultät und der Graduate School of Life Sciences (GSLS) der Universität Würzburg danke ich für die Unterstützung durch ein einjähriges Promotionsstipendium.

Meine Kollegen in der Arbeitsgruppe danke ich für ihre stets freundliche und kompetente Unterstützung meiner Arbeit. Insbesondere bei fachlichen Diskussionspunkten oder experimentellen Fragestellungen stieß ich immer auf große Hilfsbereitschaft. Dafür danke ich insbesondere Gustavo Ramos, Johannes Weirather und Benjamin Vogel von ganzem Herzen.

Denise Mathes, Edit Tanai, Anne van den Berg, Matthias Burkard, Claudia Hollmann und Nadine Gladow bin ich ebenfalls zu großem Dank verpflichtet. Laura Peters herzlichen Dank für die Durchsicht meiner Arbeit und die motivationale Unterstützung.

Ich danke außerdem Helga Wagner, Andrea Leopold, Sandra Umbenhauer und Charlotte Dienesch für die hervorragende technische Assistenz bei den Experimenten.

Ein ganz persönlicher und besonderer Dank gilt meinen Eltern, Jutta Niesel-Heinrichs und Dr. med. vet. Martin Heinrichs, denen ich diese Arbeit widme.

Während meiner gesamten Studienzeit, insbesondere aber während meines Freisemesters und meiner Arbeit im Labor, konnte ich mir ihrer bedingungslosen Unterstützung und Liebe immer gewiss sein. Sowohl mit ermutigenden als auch mit mahnenden Worten standen sie mir stets zur Seite. Meinem Vater danke ich auch für seine fachliche Beratung.

Meinem Großvater, Klaus Niesel, und seiner Frau, Hildegard Rademann-Niesel, sowie meinem Onkel, Jörg Heinrichs, danke ich für das kontinuierlich entgegengebrachte Verständnis sowie die liebevolle Zuwendung und Anteilnahme. Allen anderen Familienmitgliedern, die die Veröffentlichung dieser Arbeit leider nicht mehr erleben, danke ich für ihre frühe Förderung und Forderung meiner Person.

Mein Dank für ihre Geduld und Ermutigung bei der Fertigstellung dieser Arbeit gilt allen anderen Freundinnen und Freunden, die nicht namentlich aufgeführt sind.

Danke!

7. Publication/s

In preparation.

9. Abbreviations and definitions

2D	two-dimensional
Ab	antibody
ACE	angiotensin converting enzyme
Actb	Actin ß/b
AP	apical (in echocardiography)
APC	antigen presenting cell(s)
APS	ammonium persulfate
aqua dest.	aqua destillata = distilled water
ARDS	acute respiratory distress syndrome
ATP	adenosine triphosphate
B220/CD45R	CD45 isoform and member of the T200 glycoprotein family; pan B-cell marker
Baff	B-cell activating factor
BCA-1	B cell-attracting chemokine 1 (= CXCL13)
BCR	B-cell receptor(s)
BLC	B lymphocyte chemoattractant (= CXCL13)
BLR1	Burkitt lymphoma receptor 1 (= CXCR5)
border zone	area in-between scar and septum
B_{reg}	regulatory B cell(s)
BSA	balanced salt solution
BSS	bovine serum albumin
C3	complement component 3
cAMP	cyclic adenosine monophosphate
CAPS	N-cyclohexyl-3-aminopropanesulfonic acid
CCL*X*	CC-chemokine ligand

Ccl*X*	gene encoding CCLX
CCRX	CC-chemokine receptor
CD	cluster of differentiation
cDNA	complementary DNA
CD*X*L	ligand of CD*X*
CMV	cytomegalovirus
CTL	cytotoxic T lymphocyte(s)
CTLA-4 (CD152)	cytotoxic T lymphocyte-associated molecule 4
cTnI	cardiac troponin I
CXC	C-X-C chemokine
CXCL*X*	C-X-C motif chemokine *X*
Cxcl*X*	gene encoding CXCL*X*
CXCR*X*	C-X-C chemokine receptor type *X*
DAPI	4',6-diamidino-2-phenylindole
DC	dendritic cell(s)
DNA	deoxyribonucleic acid
DNase	deoxyribonuclease
d*X*	day X after myocardial infarction
e.g.	exempli gratia = for example
EBV	Epstein-Barr virus
ECL	enhanced chemiluminescence
ECM	extracellular matrix
EDA	end-diastolic area (in echocardiography)
ELISA	enzyme-linked immunosorbent assay
esp.	especially
et al.	et alii = and others
FACS	fluorescence-activated cell scanning = flow cytometry

F-actin	filamentous actin
FAM	6-FAM-phosphoramidit
FCS	fetal calf serum
FDC	follicular dendritic cell(s)
Foxp3	forkhead-box-protein P3
FS	fractional shortening (in echocardiography)
FSC	forward scatter
g	unit for gravity
G-actin	globular actin
GAPDH	glyceraldehyde 3-phosphate dehydrogenase
GC	germinal center(s)
H_2O	water
HCl	hydrogen chloride
HE	hematoxylin
HHV-8	human herpes virus 8
HIV	human immunodeficiency virus
HRP	horseradish peroxidase
HSV	herpes simplex virus
i.e.	id est = that is
i.p.	intraperitoneal(ly)
IFN-*X*	interferon
Ig	immunoglobulin(s)
IL-*X*	interleukin
IκBα	nuclear factor of kappa light polypeptide gene enhancer in B-cells inhibitor alpha
LAD	left anterior descending (artery) of the heart
LPS	lipopolysaccharide(s)
LT	lymphotoxin(s)

LV	left-ventricular; left ventricle
Ly6C	lymphocyte antigen 6 complex, locus C
Ly6G	lymphocyte antigen 6 complex, locus G
mAb	monoclonal antibody
MALT	mucosa-associated lymphatic tissue
MHC	major histocompatibility complex
MI	myocardial infarction
MMP *X*	matrix metalloproteinase(s)
mRNA	messenger RNA
MyD88	myeloid differentiation primary response gene 88
n	number
NaCl	sodium chloride
NC	nitrocellulose
NF-κB	nuclear factor kappa-light-chain-enhancer of activated B cells
NK (T) cells	natural killer (T) cells
NLRP3	NLR family pyrin domain containing 3
NYHA *X*	New York Heart association: scheme to categorize heart failure published by that society
p	p-value/probability value (in statistics)
PA	papillary (in echocardiography)
pAb	polyclonal antibody
PAMP	pattern-associated molecular pattern(s)
PBS	phosphate-buffered saline
PCR	polymerase chain reaction
PKA	protein kinase A
PRR	pathogen recognition receptor(s)
PSR	picrosirius red
r.o.	retroorbital(ly)

RNA	ribonucleic acid
RORC	RAR-related orphan receptor C: Gene for expression of RORγ and RORγt (transcription factors)
RPMI	cell culture medium
RT	room temperature
RT-PCR	real time polymerase chain reaction
scar	ischemically damaged heart tissue after myocardial infarction
SDS	sodiumdodecylsulfate
SDS-PAGE	sodiumdodecylsulfate polyacrylamide gel electrophoresis
SEM	standard error of the mean
septum	vital myocardium compared to infarct area (scar) after myocardial infarction (= remote zone)
sham	short form of *sham-operated*, i.e. animal operated without induction of a myocardial infarction (thoracotomy and probing of the LAD only), control group
SHM	somatic hypermutation
SSC	sideward scatter
Taq	Thermus aquatus
TBST	Tris-buffered saline with Tween 20
TCR	T-cell receptor(s)
Temed	tetramethylethylendiamine
Tfh cell(s)	T follicular helper cell(s)
TGF-*X*	transforming growth factor
Th1/2 cell(s)	T helper cell(s) 1/2
Th17 cell(s)	IL-17 producing T helper cell(s)
TIR	toll-interleukin-1 receptor, the cytoplasmic domain of TLR4
TIRAP (Mal)	toll-interleukin-1 receptor domain containing adaptor protein
TLR	toll-like receptor(s)
TNF-*X*	tumor necrosis factor

TRAM	translocating chain-associated membrane protein
T_{reg}	regulatory T cell(s)
TRIF (TICAM-1)	TIR-domain-containing adapter-inducing interferon-β
Tris	tris(2-aminoethyl)amine
v	velocity
vol.	volume
VZV	varicella-zoster virus
x	times/fold

10. List of references

1. Iwasaki, A. & Medzhitov, R. Control of adaptive immunity by the innate immune system. *Nat. Immunol.* **16,** 343–353 (2015).
2. Delves, P. J. & Roitt, I. M. The Immune System. *N. Engl. J. Med.* **343,** 37–49 (2000).
3. Theilacker, C. *et al.* Overwhelming Postsplenectomy Infection: A Prospective Multicenter Cohort Study. *Clin. Infect. Dis.* **62,** 871–878 (2016).
4. Antman, K. & Chang, Y. Kaposi's Sarcoma. *N. Engl. J. Med.* **342,** 1027–1038 (2000).
5. WHO | The top 10 causes of death. *WHO* Available at: http://www.who.int/mediacentre/factsheets/fs310/en/. (Accessed: 19th September 2015)
6. Libby, P. Inflammation in atherosclerosis. *Nature* **420,** 868–874 (2002).
7. Shen, H., Kreisel, D. & Goldstein, D. R. Processes of Sterile Inflammation. *J. Immunol.* **191,** 2857–2863 (2013).
8. Staat & Gesellschaft - Todesursachen - 2012: Anstieg der Todesfälle im Vergleich zum Vorjahr um 2 % - Statistisches Bundesamt (Destatis). Available at: https://www.destatis.de/DE/ZahlenFakten/GesellschaftStaat/Gesundheit/Todesursachen/Aktuell.html. (Accessed: 22nd May 2014)
9. Michels, K. B. & Yusuf, S. Does PTCA in Acute Myocardial Infarction Affect Mortality and Reinfarction Rates? A Quantitative Overview (Meta-Analysis) of the Randomized Clinical Trials. *Circulation* **91,** 476–485 (1995).
10. Tsiantoulas, D., Diehl, C. J., Witztum, J. L. & Binder, C. J. B cells and humoral immunity in atherosclerosis. *Circ. Res.* **114,** 1743–1756 (2014).
11. Gale, R. P. Development of the immune system in human fetal liver. *Thymus* **10,** 45–56 (1987).
12. Hayward, A. R. The human fetus and newborn: development of the immune response. *Birth Defects Orig. Artic. Ser.* **19,** 289–294 (1983).
13. Niewiesk, S. Maternal Antibodies: Clinical Significance, Mechanism of Interference with Immune Responses, and Possible Vaccination Strategies. *Front. Immunol.* **5,** (2014).
14. Bogaert, D., Weinberger, D., Thompson, C., Lipsitch, M. & Malley, R. Impaired Innate and Adaptive Immunity to Streptococcus pneumoniae and Its Effect on Colonization in an Infant Mouse Model. *Infect. Immun.* **77,** 1613–1622 (2009).
15. Levy, O. Innate immunity of the newborn: basic mechanisms and clinical correlates. *Nat. Rev. Immunol.* **7,** 379–390 (2007).
16. Holladay, S. D. & Smialowicz, R. J. Development of the murine and human immune system: differential effects of immunotoxicants depend on time of exposure. *Environ. Health Perspect.* **108,** 463–473 (2000).
17. Tavassoli, M. Embryonic and fetal hemopoiesis: an overview. *Blood Cells* **17,** 269–281; discussion 282-286 (1991).
18. Tavassoli M, Yoffey JM. Bone marrow: structure and function. - 2009 - Scandinavian Journal of Haematology - Wiley Online Library. Available at: http://onlinelibrary.wiley.com/doi/10.1111/j.1600-0609.1984.tb01701.x/abstract. (Accessed: 9th January 2016)
19. Adkins, B. *et al.* Early events in T-cell maturation. *Annu. Rev. Immunol.* **5,** 325–365 (1987).
20. Osmond, D. G., Rolink, A. & Melchers, F. Murine B lymphopoiesis: towards a unified model. *Immunol. Today* **19,** 65–68 (1998).

21. Berrut, G. & de Decker, L. Immunosenescence: a review. *Geriatr. Psychol. Neuropsychiatr. Vieil.* **13,** 7–14 (2015).
22. Janeway, C. A., Jr & Medzhitov, R. Innate immune recognition. *Annu. Rev. Immunol.* **20,** 197–216 (2002).
23. Medzhitov, R. Recognition of microorganisms and activation of the immune response. *Nature* **449,** 819–826 (2007).
24. Kumar, H., Kawai, T. & Akira, S. Pathogen recognition by the innate immune system. *Int. Rev. Immunol.* **30,** 16–34 (2011).
25. Hoebe, K., Janssen, E. & Beutler, B. The interface between innate and adaptive immunity. *Nat. Immunol.* **5,** 971–974 (2004).
26. Kawai, T. & Akira, S. TLR signaling. *Semin. Immunol.* **19,** 24–32 (2007).
27. Kumar, H., Kawai, T. & Akira, S. Toll-like receptors and innate immunity. *Biochem. Biophys. Res. Commun.* **388,** 621–625 (2009).
28. Sun, Z. & Andersson, R. NF-kappaB activation and inhibition: a review. *Shock Augusta Ga* **18,** 99–106 (2002).
29. Ichinohe, T., Pang, I. K. & Iwasaki, A. Influenza virus activates inflammasomes via its intracellular M2 ion channel. *Nat. Immunol.* **11,** 404–410 (2010).
30. Beutler, B. & Rietschel, E. T. Innate immune sensing and its roots: the story of endotoxin. *Nat. Rev. Immunol.* **3,** 169–176 (2003).
31. Raetz, C. R. H. & Whitfield, C. Lipopolysaccharide endotoxins. *Annu. Rev. Biochem.* **71,** 635–700 (2002).
32. Poltorak, A. *et al.* Defective LPS signaling in C3H/HeJ and C57BL/10ScCr mice: mutations in Tlr4 gene. *Science* **282,** 2085–2088 (1998).
33. Buchta, C. M. & Bishop, G. A. Toll-like receptors and B cells: functions and mechanisms. *Immunol. Res.* (2014). doi:10.1007/s12026-014-8523-2
34. Manjarrez-Orduño, N., Quách, T. D. & Sanz, I. B cells and immunological tolerance. *J. Invest. Dermatol.* **129,** 278–288 (2009).
35. Jr, C. A. J. *et al. Immunobiology*. (Garland Science, 2001).
36. CD8+ T Cells | Bitesized Immunology. Available at: http://bitesized.immunology.org/cells/cd8-t-cells/. (Accessed: 19th March 2016)
37. Parker, D. C. T Cell-Dependent B Cell Activation. *Annu. Rev. Immunol.* **11,** 331–360 (1993).
38. Charles A Janeway, J., Travers, P., Walport, M. & Shlomchik, M. J. B-cell activation by armed helper T cells. (2001).
39. Poo, W. J., Conrad, L. & Janeway, C. A. Receptor-directed focusing of lymphokine release by helper T cells. *Nature* **332,** 378–380 (1988).
40. Brown, M. A. IL-4 Production by T Cells: You Need a Little to Get a Lot. *J. Immunol.* **181,** 2941–2942 (2008).
41. Wykes, M. Why do B cells produce CD40 ligand? *Immunol. Cell Biol.* **81,** 328–331 (2003).
42. OMIM Entry - * 300292 - FORKHEAD BOX P3; FOXP3. Available at: http://www.omim.org/entry/300292. (Accessed: 21st March 2016)
43. Guo, L., Zheng, B. & Han, S. Constitutive expression of Foxp3 in conventional T cells reduces cellular proliferation and alleviates autoimmune arthritis. *J. Immunol.* **182,** 137.25 (2009).
44. FOXP3 Gene - GeneCards | FOXP3 Protein | FOXP3 Antibody. Available at: http://www.genecards.org/cgi-bin/carddisp.pl?gene=FOXP3. (Accessed: 14th February 2016)
45. Zhou, L. *et al.* TGF-beta-induced Foxp3 inhibits T(H)17 cell differentiation by antagonizing RORgammat function. *Nature* **453,** 236–240 (2008).
46. Toker, A. & Huehn, J. To be or not to be a Treg cell: lineage decisions controlled by epigenetic mechanisms. *Sci. Signal.* **4,** pe4 (2011).

47. Berger, A. Th1 and Th2 responses: what are they? *BMJ* **321,** 424 (2000).
48. Korn, T., Bettelli, E., Oukka, M. & Kuchroo, V. K. IL-17 and Th17 Cells. *Annu. Rev. Immunol.* **27,** 485–517 (2009).
49. Sutton, M. G. S. J. & Sharpe, N. Left Ventricular Remodeling After Myocardial Infarction Pathophysiology and Therapy. *Circulation* **101,** 2981–2988 (2000).
50. Torre-Amione, G. *et al.* Results of a non-specific immunomodulation therapy in chronic heart failure (ACCLAIM trial): a placebo-controlled randomised trial. *The Lancet* **371,** 228–236 (2008).
51. Pfeffer, M. A. & Braunwald, E. Ventricular remodeling after myocardial infarction. Experimental observations and clinical implications. *Circulation* **81,** 1161–1172 (1990).
52. Liao, Y.-H. & Cheng, X. Autoimmunity in myocardial infarction. *Int. J. Cardiol.* **112,** 21–26 (2006).
53. Dellas, C. *Last Minute Pharmakologie*. (Elsevier, Urban & Fischer, 2011).
54. Yan, X. *et al.* Temporal dynamics of cardiac immune cell accumulation following acute myocardial infarction. *J. Mol. Cell. Cardiol.* **62,** 24–35 (2013).
55. Weirather, J. *et al.* Foxp3+CD4+ T Cells Improve Healing after Myocardial Infarction by Modulating Monocyte/Macrophage Differentiation. *Circ. Res.* (2014). doi:10.1161/CIRCRESAHA.115.303895
56. Zouggari, Y. *et al.* B lymphocytes trigger monocyte mobilization and impair heart function after acute myocardial infarction. *Nat. Med.* **19,** 1273–1280 (2013).
57. Bönner, F., Borg, N., Burghoff, S. & Schrader, J. Resident cardiac immune cells and expression of the ectonucleotidase enzymes CD39 and CD73 after ischemic injury. *PloS One* **7,** e34730 (2012).
58. Ait-Oufella, H. *et al.* B cell depletion reduces the development of atherosclerosis in mice. *J. Exp. Med.* **207,** 1579–1587 (2010).
59. Ramos, G. C. *et al.* The autoimmune nature of post-infarct myocardial healing: oral tolerance to cardiac antigens as a novel strategy to improve cardiac healing. *Autoimmunity* **45,** 233–244 (2012).
60. Isoproterenol: Indications, Side Effects, Warnings - Drugs.com. Available at: http://www.drugs.com/cdi/isoproterenol.html. (Accessed: 21st February 2016)
61. Rona, G., Chappel, C. I., Balazs, T. & Gaudry, R. An infarct-like myocardial lesion and other toxic manifestations produced by isoproterenol in the rat. *AMA Arch. Pathol.* **67,** 443–455 (1959).
62. Li, J. *et al.* Mucosal tolerance induction in autoimmune myocarditis and myocardial infarction. *Int. J. Cardiol.* **162,** 245–252 (2013).
63. Frenkel, D. *et al.* Nasal vaccination with troponin reduces troponin specific T-cell responses and improves heart function in myocardial ischemia-reperfusion injury. *Int. Immunol.* **21,** 817–829 (2009).
64. Frey, A. *et al.* Early citalopram treatment increases mortality due to left ventricular rupture in mice after myocardial infarction. *J. Mol. Cell. Cardiol.* (2016). doi:10.1016/j.yjmcc.2016.07.002
65. Courties, G., Moskowitz, M. A. & Nahrendorf, M. The innate immune system after ischemic injury: lessons to be learned from the heart and brain. *JAMA Neurol.* **71,** 233–236 (2014).
66. Hofmann, U. *et al.* Activation of CD4+ T lymphocytes improves wound healing and survival after experimental myocardial infarction in mice. *Circulation* **125,** 1652–1663 (2012).
67. Iwata, Y. *et al.* CD19, a response regulator of B lymphocytes, regulates wound healing through hyaluronan-induced TLR4 signaling. *Am. J. Pathol.* **175,** 649–660 (2009).

68. Maseda, D., Bonami, R. H. & Crofford, L. J. Regulation of B lymphocytes and plasma cells by innate immune mechanisms and stromal cells in rheumatoid arthritis. *Expert Rev. Clin. Immunol.* **10,** 747–762 (2014).
69. Bao, Y. & Cao, X. The immune potential and immunopathology of cytokine-producing B cell subsets: A comprehensive review. *J. Autoimmun.* (2014). doi:10.1016/j.jaut.2014.04.001
70. Yardeni, T., Eckhaus, M., Morris, H. D., Huizing, M. & Hoogstraten-Miller, S. Retro-orbital injections in mice. *Lab Anim.* **40,** 155–160 (2011).
71. Kaya, E. *et al.* Amanitin and phallotoxin concentration in Amanita phalloides var. alba mushroom. *Toxicon* **76,** 225–233 (2013).
72. PHALLOIDIN - National Library of Medicine HSDB Database. Available at: https://toxnet.nlm.nih.gov/cgi-bin/sis/search/a?dbs+hsdb:@term+@DOCNO+3524. (Accessed: 23rd August 2016)
73. Vogel, B., Siebert, H., Hofmann, U. & Frantz, S. Determination of collagen content within picrosirius red stained paraffin-embedded tissue sections using fluorescence microscopy. *MethodsX* **2,** 124–134 (2015).
74. Fischer, A. H., Jacobson, K. A., Rose, J. & Zeller, R. Hematoxylin and eosin staining of tissue and cell sections. *CSH Protoc.* **2008,** pdb.prot4986 (2008).
75. Junqueira, L. C., Bignolas, G. & Brentani, R. R. Picrosirius staining plus polarization microscopy, a specific method for collagen detection in tissue sections. *Histochem. J.* **11,** 447–455 (1979).
76. Coffman, R. L. & Weissman, I. L. B220: a B cell-specific member of the T200 glycoprotein family. *Nature* **289,** 681–683 (1981).
77. Cerutti, A., Cols, M. & Puga, I. Marginal zone B cells: virtues of innatelike antibody-producing lymphocytes. *Nat. Rev. Immunol.* **13,** 118–132 (2013).
78. Takemura, S. *et al.* Lymphoid neogenesis in rheumatoid synovitis. *J. Immunol. Baltim. Md 1950* **167,** 1072–1080 (2001).
79. Tangye, S. G. To B1 or not to B1: that really is still the question! *Blood* **121,** 5109–5110 (2013).
80. Baumgarth, N. The double life of a B-1 cell: self-reactivity selects for protective effector functions. *Nat. Rev. Immunol.* **11,** 34–46 (2011).
81. Zabel, M. D. & Weis, J. H. Cell-specific regulation of the CD21 gene. *Int. Immunopharmacol.* **1,** 483–493 (2001).
82. Smedbakken, L. M. *et al.* Increased levels of the homeostatic chemokine CXCL13 in human atherosclerosis - Potential role in plaque stabilization. *Atherosclerosis* **224,** 266–273 (2012).
83. Kowarik, M. C. *et al.* CXCL13 is the major determinant for B cell recruitment to the CSF during neuroinflammation. *J. Neuroinflammation* **9,** 93 (2012).
84. Krumbholz, M. *et al.* Chemokines in multiple sclerosis: CXCL12 and CXCL13 up-regulation is differentially linked to CNS immune cell recruitment. *Brain J. Neurol.* **129,** 200–211 (2006).
85. Kramer, J. M., Klimatcheva, E. & Rothstein, T. L. CXCL13 is elevated in Sjogren's syndrome in mice and humans and is implicated in disease pathogenesis. *J. Leukoc. Biol.* (2013). doi:10.1189/jlb.0113036
86. Schmutz, C. *et al.* Chemokine receptors in the rheumatoid synovium: upregulation of CXCR5. *Arthritis Res. Ther.* **7,** R217-229 (2005).
87. Nagasawa, T. CXC chemokine ligand 12 (CXCL12) and its receptor CXCR4. *J. Mol. Med. Berl. Ger.* **92,** 433–439 (2014).
88. Comerford, I. *et al.* A myriad of functions and complex regulation of the CCR7/CCL19/CCL21 chemokine axis in the adaptive immune system. *Cytokine Growth Factor Rev.* **24,** 269–283 (2013).

89. CXCL13 (mouse). Available at: http://www.phosphosite.org/proteinAction?id=3290802&showAllSites=true. (Accessed: 14th September 2016)
90. Frantz, S. *et al.* Monocytes/macrophages prevent healing defects and left ventricular thrombus formation after myocardial infarction. *FASEB J. Off. Publ. Fed. Am. Soc. Exp. Biol.* **27,** 871–881 (2013).
91. Finch, D. K., Ettinger, R., Karnell, J. L., Herbst, R. & Sleeman, M. A. Effects of CXCL13 inhibition on lymphoid follicles in models of autoimmune disease. *Eur. J. Clin. Invest.* **43,** 501–509 (2013).
92. Serbina, N. V., Shi, C. & Pamer, E. G. Monocyte-mediated immune defense against murine Listeria monocytogenes infection. *Adv. Immunol.* **113,** 119–134 (2012).
93. Dutta, P. & Nahrendorf, M. Monocytes in myocardial infarction. *Arterioscler. Thromb. Vasc. Biol.* **35,** 1066–1070 (2015).
94. Kim, S. S., Kirou, K. A. & Erkan, D. Belimumab in systemic lupus erythematosus: an update for clinicians. *Ther. Adv. Chronic Dis.* **3,** 11–23 (2012).
95. Kaplan, B., Kopyltsova, Y., Khokhar, A., Lam, F. & Bonagura, V. Rituximab and immune deficiency: case series and review of the literature. *J. Allergy Clin. Immunol. Pract.* **2,** 594–600 (2014).
96. Bio-Rad. B Cells - Function, Activation, Lineage & Markers. *Bio-Rad* Available at: https://www.bio-rad-antibodies.com/b-cell-function-activation-lineage-marker-antibody.html. (Accessed: 25th March 2018)
97. Halvorsen, B. *et al.* Activated platelets promote increased monocyte expression of CXCR5 through prostaglandin E2-related mechanisms and enhance the anti-inflammatory effects of CXCL13. *Atherosclerosis* **234,** 352–359 (2014).
98. Klein, U. & Dalla-Favera, R. Germinal centres: role in B-cell physiology and malignancy. *Nat. Rev. Immunol.* **8,** 22–33 (2008).
99. Wang, X. *et al.* Follicular dendritic cells help establish follicle identity and promote B cell retention in germinal centers. *J. Exp. Med.* **208,** 2497–2510 (2011).
100. Förster, R. *et al.* A putative chemokine receptor, BLR1, directs B cell migration to defined lymphoid organs and specific anatomic compartments of the spleen. *Cell* **87,** 1037–1047 (1996).
101. Garraud, O. *et al.* Revisiting the B-cell compartment in mouse and humans: more than one B-cell subset exists in the marginal zone and beyond. *BMC Immunol.* **13,** 63 (2012).
102. Hargreaves, D. C. *et al.* A coordinated change in chemokine responsiveness guides plasma cell movements. *J. Exp. Med.* **194,** 45–56 (2001).
103. McDonnell, M. *et al.* Systemic Toll-like receptor ligands modify B-cell responses in human inflammatory bowel disease. *Inflamm. Bowel Dis.* **17,** 298–307 (2011).
104. Chtanova, T. *et al.* T follicular helper cells express a distinctive transcriptional profile, reflecting their role as non-Th1/Th2 effector cells that provide help for B cells. *J. Immunol. Baltim. Md 1950* **173,** 68–78 (2004).
105. Crotty, S. T follicular helper cell differentiation, function, and roles in disease. *Immunity* **41,** 529–542 (2014).
106. Simpson, N. *et al.* Expansion of circulating T cells resembling follicular helper T cells is a fixed phenotype that identifies a subset of severe systemic lupus erythematosus. *Arthritis Rheum.* **62,** 234–244 (2010).
107. Morita, R. *et al.* Human blood CXCR5(+)CD4(+) T cells are counterparts of T follicular cells and contain specific subsets that differentially support antibody secretion. *Immunity* **34,** 108–121 (2011).

108. He, J. *et al.* Circulating precursor CCR7(lo)PD-1(hi) CXCR5$^+$ CD4$^+$ T cells indicate Tfh cell activity and promote antibody responses upon antigen reexposure. *Immunity* **39,** 770–781 (2013).
109. Spolski, R. & Leonard, W. J. Interleukin-21: a double-edged sword with therapeutic potential. *Nat. Rev. Drug Discov.* **13,** 379–395 (2014).
110. Peterson, J. D. & Chan, L. S. Effectiveness and side effects of anti-CD20 therapy for autoantibody-mediated blistering skin diseases: A comprehensive survey of 71 consecutive patients from the Initial use to 2007. *Ther. Clin. Risk Manag.* **5,** 1–7 (2009).
111. Cyster, J. G. *et al.* Follicular stromal cells and lymphocyte homing to follicles. *Immunol. Rev.* **176,** 181–193 (2000).
112. Legler, D. F. *et al.* B cell-attracting chemokine 1, a human CXC chemokine expressed in lymphoid tissues, selectively attracts B lymphocytes via BLR1/CXCR5. *J. Exp. Med.* **187,** 655–660 (1998).
113. Carlsen, H. S., Baekkevold, E. S., Morton, H. C., Haraldsen, G. & Brandtzaeg, P. Monocyte-like and mature macrophages produce CXCL13 (B cell-attracting chemokine 1) in inflammatory lesions with lymphoid neogenesis. *Blood* **104,** 3021–3027 (2004).
114. Kobayashi, S. *et al.* A distinct human CD4+ T cell subset that secretes CXCL13 in rheumatoid synovitis. *Arthritis Rheum.* (2013). doi:10.1002/art.38173
115. Männ, L., Klingberg, A., Gunzer, M. & Hasenberg, M. Quantitative Visualization of Leukocyte Infiltrate in a Murine Model of Fulminant Myocarditis by Light Sheet Microscopy. *J. Vis. Exp. JoVE* (2017). doi:10.3791/55450
116. Yang, M., Rui, K., Wang, S. & Lu, L. Regulatory B cells in autoimmune diseases. *Cell. Mol. Immunol.* **10,** 122–132 (2013).
117. Gruver, A., Hudson, L. & Sempowski, G. Immunosenescence of ageing. *J. Pathol.* **211,** 144–156 (2007).
118. Ramos, G. C. *et al.* Myocardial aging as a T-cell-mediated phenomenon. *Proc. Natl. Acad. Sci. U. S. A.* **114,** E2420–E2429 (2017).

Other source:
Miamed, Amboss, Miamed GmbH, Köln: https://www.miamed.de/
(last accessed: 28/03/2018)

11. List of figures

12. Affidavit/Eidesstattliche Erklärung

I hereby confirm that my thesis entitled “Myocardial B-cell infiltration after LAD occlusion in mice is driven by CXCL13“ is the result of my own work. I did not receive any help or support from commercial consultants. All sources and/or materials applied are listed and specified in the thesis.

Furthermore, I confirm that this thesis has not yet been submitted as part of another examination process neither in identical nor in similar form.

Hiermit erkläre ich an Eides statt, die Dissertation „Die Infiltration des Myokards durch B-Lymphozyten nach Ligatur der linken Koronararterie im Mausmodell wird durch CXCL13 verursacht“ eigenständig, d.h. insbesondere selbstständig und ohne Hilfe eines kommerziellen Promotionsberaters, angefertigt und keine anderen als die von mir angegebenen Quellen und Hilfsmittel verwendet zu haben.

Ich erkläre außerdem, dass die Dissertation weder in gleicher noch in ähnlicher Form bereits in einem anderen Prüfungsverfahren vorgelegen hat.

Würzburg, 28/03/2018